PALEOENVRIONMENTAL RECONSTRUCTION OF THE BRADY SOIL IN THE NEBRASKA LOESS UPLANDS USING BIOSILICATE AND BIOTURBATION ANALYSES

By
Terri L. Woodburn

Submitted to the Department of Geography and the
faculty of the Graduate School of the University of Kansas
in partial fulfillment of the requirements for the degree of
Doctor of Philosophy.

Committee members:

_____
William C. Johnson, Chair

_____
Daniel R. Hirmas

_____
Stephen T. Hasiotis

_____
Steven R. Bozarth

_____
Kendra K. McLauchlan

Date defended: August 1, 2013

The Dissertation Committee for Terri L. Woodburn certifies
that this is the approved version of the following dissertation:

PALEOENVRIONMENTAL RECONSTRUCTION OF THE BRADY SOIL IN THE NEBRASKA LOESS UPLANDS USING BIOSILICATE AND BIOTURBATION ANALYSES

Committee:

William C. Johnson, Chair

Daniel R. Hirmas

Stephen T. Hasiotis

Steven R. Bozarth

Kendra K. McLauchlan

Date approved: December 19, 2014

Abstract

This dissertation takes a multiple-proxy approach to a paleoenvironmental reconstruction of the Holocene—Pleistocene Transition represented by the Brady Soil in the central Great Plains. To better understand this dynamic time of climate change, and to overcome the limitations of previous analyses using stable carbon isotope data, this study employs phytoliths to provide specific information on paleovegetation communities and quantitative shifts of plant taxa. Climatic indices based on both short- and large-cell phytolith frequencies add needed data on shifts of relative temperature (C_3:C_4 Grassland Ratio), water stress on plants (Bulliform Index), and soil moisture (from a proposed Soil Moisture Index). Analysis of short cell phytoliths reveals quantitative plant taxa shifts from Pooideae (C_3) dominant grasses, with relatively large numbers of arboreal dicot spheres and a few Cyperaceae (sedge) present in a savannah or open woodland setting in the Bølling-Allerød climatic period (~14.6 ka to 12.9 ka), to a mixed, open grassland of Chloridoideae (C_4) and Pooideae (C_3) in the early Holocene. *Stipa*-type Pooideae, a cool-season grass preferring drier soil conditions, marks the onset of the Younger Dryas (~12.9 ka to 11.7 ka), which was previously not revealed in $\delta^{13}C$ analysis.

Brady Soil bioturbation was examined to provide a new proxy for paleoenvironmental conditions in addition to determining the effect of bioturbation particular to this soil on sediment transportation through the profile. Through macro- and micromorphology, particle size, soil color, and phytolith signatures, it was determined that invertebrate activity (primarily by cicada nymphs (Cicadidae) or burrower bugs (Cydnidae) of the *Naktodemasis bowni* ichnotaxon) was highly localized (diffusive mixing). Similar modern burrowers tend to be correlated with woody vegetation necessary throughout their lifecycle. Increased activity of cicada within the Bkb horizon corroborates phytolith reconstruction, indicating savannah to open woodland conditions during this time of Brady Soil pedogenesis. Non-local (advective) mixing is also prevalent due to vertebrate activity. Burrow and chamber construction, size parameters, and scratch traces indicate activity by prairie dog (*Cynomys* sp.) or ground squirrel (*Spermophilus* sp.).

Acknowledgements

I would like to convey my gratitude to the numerous people who supported me during my research and writing process, without whom, this dissertation would not have been possible. First and foremost, I thank my advisor, Dr. William Johnson, for his patient guidance, excellent field instruction over the years, and careful editing and advice that has improved my writing skills. Bill's mentoring during my graduate career has provided me with the skills necessary to continue into a future in academia. I am truly fortunate to have had the opportunity to work with and learn from him and I greatly appreciate his efforts.

I thank my committee members, Stephen Hasiotis, Dan Hirmas, Steven Bozarth, and Kendra McLauchlan for their helpful suggestions, advice, and editorial comments for the dissertation. I am grateful to each of my committee members for improving my knowledge of pedogenesis, ichnology, and phytolith analysis through courses, discussions, and fieldwork.

I have been privileged to share my PhD experience with Alan Halfen who was a great sounding board and collaborator. I am thankful for the assistance and friendship he provided through this process, as well as his adept Adobe Illustrator abilities. Alan, along with Robin Moore, contributed to this project through sample collection and thin-section production. Also, a special thanks goes to the landowners of the Old Wauneta Roadcut site for allowing multiple visits for sampling over the years, and to Joe Mason who originally found the site and shared it.

Research support was provided through the University of Kansas (KU) General Research Fund and the Kollmorgen Fellowship Award from the KU Geography Department. I am also thankful to the KU Geography Department, the Kansas Geological Survey, and Bill Johnson for providing me with the opportunity for graduate teaching and research assistantships that helped support me through the PhD program.

Finally, I am forever indebted to my husband Brent for his support and patience over the years. Without him, I would not have had the opportunity to follow my passion and pursue a PhD in geography.

Table of Contents

Chapter 1. Introduction

The goal of this dissertation is to produce and interpret new proxy data in order to reconstruct a comprehensive paleoenvironmental record for the Brady Soil, a ubiquitous buried paleosol within the central Great Plains. The dissertation includes multiple proxy records and environmental interpretations presented in two chapters that are written as individual papers to be submitted to peer-review journals. The chapters are separated into the topics of soil biota activity and vegetation dynamics during the Pleistocene—Holocene transition (PHT) as recorded by Brady Soil pedogenesis.

Climate conditions during the final stages of deglaciation at the PHT are characterized by the occurrence of frequent and rapid fluctuations (Alley, 2000; Zielinski and Mershon, 1997). Understanding these abrupt climate change events is of considerable interest to studies of climate effects on human and animal populations across this time period (Holliday et al., 2011), and to those modeling future scenarios of similar climate change triggers (Alley, 2000). Terrestrial data for the Pleistocene-Holocene transition from interior North America lack the detail needed to produce a complete paleoenvironmental and paleoclimate reconstruction for this interval of pronounced climate change (Mason et al., 2008; Holliday et al., 2011). In the central Great Plains, this transitional period coincides with an interval of soil formation—the Brady Soil—developing between ~14.7—9 ka (Mason et al., 2008) during terminal deposition of the Last Glacial Maximum Peoria Loess. Focusing on the Brady Soil of an upland loess plateau in southwestern Nebraska, this study improves the understanding of climate events through the use of relatively high-resolution phytolith analysis. This analysis provides specific information on paleovegetation communities and quantitative temporal shifts of plant taxa, in addition to climate indices produced from phytolith frequencies. Climate indices are calculated to identify discrete drought periods,

evapotranspiration rate changes, and precipitation and soil moisture availability. Micromorphology of soil matrix and burrow fill thin sections, paired with soil macromorphology, L*a*b color parameters, particle size distribution, and phytolith assemblages are utilized to assess the scale of disturbance within a soil due to floral and faunal bioturbation.

Previous research of the PHT in the central Great Plains shows a general trend of warming and drying into the Holocene based on (1) slight shifts from C_3- to C_4-dominant vegetation in stable carbon isotope analyses; (2) illuvial clay in the Brady B horizon indicating greater moisture availability compared to the overlying Holocene paleosols; and (3) a decrease in burrow density into the Holocene (e.g., Johnson and Willey, 2000; Mason and Kuzila, 2000; Jacobs and Mason, 2004; Miao et al., 2007). Previous proxy data, however, do not provide the necessary detail for full environmental characterizations of this interval, especially for the Younger Dryas time period, and do not take into account the full ramifications of bioturbation on the stratigraphic integrity of proxy data. Bioturbation studies can explain the spatial distribution and transportation of material through the soil profile. Vertical mixing of sediment may create discrepancies in age determination and proxy analyses, such as stable carbon isotopes, organic carbon, or grain-size distributions (e.g., Stein, 1983; Grave and Kealhofer, 1999; Lim et al., 2007; Halfen and Hasiotis, 2010). The Brady Soil has abundant, well-preserved trace fossils that are used in the absence of body fossils to identify tracemakers through comparisons with burrow size and architecture of extant species (Hasiotis, 2002, 2003; Smith et al., 2008; Tobin, 2004). These ichnofossils record biota responses to environmental conditions documented in the PHT, and also provide supplementary data that can corroborate conclusions regarding vegetation assemblages (Jacobs and Mason, 2004; Smith and Hasiotis, 2008).

References

Alley, R.B., 2000. The Younger Dryas cold interval as viewed from central Greenland. Quaternary Science Review, 19: 213-226.

Grave, P. and Kealhofer, L., 1999. Assessing bioturbation in archaeological sediments using soil morphology and phytolith analysis. Journal of Archaeological Science, 26(10): 1239-1248.

Halfen, A.F., and Hasiotis, S.T., 2010. Neoichnological study of traces and burrowing behaviors of the western harvester ant *Pogonomymex occidentalis* (Insecta: Hymenoptera: Formicidae): paleopedogenic and paleoecological implications. PALAIOS, 25(11); 703-720.

Hasiotis, S.T., 2002. Continental Trace Fossils. SEPM Short Course Notes, 51, Tulsa, Oklahoma, 134 pp.

Hasiotis, S.T., 2003. Complex ichnofossils of solitary and social soil organisms: understanding their evolution and roles in terrestrial paleoecosystems. Palaeogeography, Palaeoclimatology, Palaeoecology, 192(1-4): 259-320.

Holliday, V.T., Meltzer, D.J. and Mandel, R., 2011. Stratigraphy of the Younger Dryas Chronozone and paleoenvironmental implications: Central and Southern Great Plains. Quaternary International, 242(2): 520-533.

Jacobs, P.M. and Mason, J.A., 2004. Paleopedology of soils in thick Holocene loess, Nebraska, USA. Revista Mexicana de Ciencias Geologicas, 21(1): 54-70.

Johnson, W.C., and Willey, K.L., 2000. Isotopic and rock magnetic expression of environmental change at the Pleistocene-Holocene transition in the central Great Plains. Quaternary International, 67: 89-106.

Lim, H.S., Lee, Y., Yi, S., Kim, C., Chung, C., Lee, H., and Choi, J.H., 2007. Vertebrate burrows in late Pleistocene paleosols at Korean Palaeolithic sites and their significance as a stratigraphic marker. Quaternary Research, 68(2): 213-219.

Mason, J.A., and Kuzila, M.S., 2000. Episodic Holocene loess deposition in central Nebraska. Quaternary International, 67: 119-131.

Mason, J.A., Miao, X., Hanson, P.R., Johnson, W.C., Jacobs, P.M., and Goble, R.J., 2008. Loess record of the Pleistocene-Holocene transition on the northern and central Great Plains, USA. Quaternary Science Review, 27: 1772-1783.

Miao, X., Mason, J.A., Johnson, W.C., and Wand, H., 2007. High-resolution proxy record of Holocene climate from a loess section in Southwestern Nebraska, USA. Palaeogeography, Palaeoclimatology, Palaeoecology, 245: 368-381.

Smith, J.J. and Hasiotis, S.T., 2008. Traces and burrowing behaviors of the cicada nymph *Cicadetta calliope*: Neoichnology and paleoecological significance of extant soil-dwelling insects. PALAIOS, 23(8): 503-513.

Smith, J.J., Hasiotis, S.T., Kraus, M.J. and Woody, D.T., 2008. *Naktodemasis bowni:* New ichnogenus and ichnospecies for adhesive meniscate burrows (AMB), and paleoenvironmental implications, Paleogene Willwood Formation, Bighorn Basin, Wyoming. Journal of Paleontology, 82(2): 267-278.

Stein, J.K., 1983. Earthworm Activity: A Source of Potential Disturbance of Archaeological Sediments. American Antiquity, 48(2): 277-289.

Tobin, R.J., 2004. Ichnology of a late Pleistocene ichnofabric, Nebraska, USA. Palaeogeography Palaeoclimatology Palaeoecology, 215(1-2): 111-123.

Zielinski, G.A. and Mershon, G.R., 1997. Paleoenvironmental implications of the insoluble microparticle record in the GISP2 (Greenland) ice core during the rapidly changing climate of the Pleistocene-Holocene transition. Geological Society of America Bulletin, 109(5): 547-559.

Chapter 2. Assessing mixing by bioturbation in the Brady Soil using micromorphology and phytolith analysis

Woodburn, Terri L., Hasiotis, Stephen T., and Johnson, William C. Assessing mixing by bioturbation in the Brady Soil using micromorphology and phytolith analysis. *PALAIOS.*

Abstract

The Old Wauneta Roadcut site in southwestern Nebraska exhibits a 1.2 meter-thick exposure of the Brady Soil, a buried paleosol that formed within loess during the Pleistocene-Holocene transition. The Brady Soil is an accretionary soil within the uppermost part of the Last Glacial Maximum Peoria Loess. Excavation of the loess-paleosol sequence has revealed considerable bioturbation by plant roots, invertebrates, and small vertebrates. A bioturbation index of 4 for the Brady Ab, ABb, and Bkb horizons denotes horizons with high trace density with common overlap (Taylor and Goldring, 1993). Bioturbation was not restricted to a single time period, but occurred continually throughout soil development, as evidenced by differing sediment fills and crosscutting relationships. At the base of the solum, the Bkb horizon exhibits an increased illuvial clay and carbonate content, and contains extensive, small (~2cm wide), miniscate backfilled burrows (ichnotaxon *Naktodemasis bowni*) typically produced by cicada nymphs (Cicadidae) and beetle (Scarabaeidae) larvae. The most stable period of the Brady Soil is expressed by the dark (9.8 YR 4/1), thick Ab horizon. This is overlain by an ACb horizon, where soil formation was being extinguished by the onset of Holocene-age Bignell Loess deposition. Within the upper solum and Bignell Loess, a shift in biota activity occurs as indicated by the large burrow (6-12 cm wide) and

chamber (30-40 cm wide) systems observed. Trace sizes suggest that a burrowing rodent, such as the prairie dog (*Cynomys* sp.) or ground squirrel (*Spermophilus* sp.), was responsible for their creation.

Micromorphology was used to differentiate soil features produced by faunal and floral activity from features produced by pedologic processes through the identification and classification of granular and spongy microstructures indicative of excrement, calcitic biospheroids, infilling, meniscate backfilling, and channel microstructures. Based on particle size, L*a*b color, and phytolith signals, rodent burrows are sources of non-local (advective) mixing with infill from upper profile units, but are typically easy to detect and can be avoided during sampling. *N. bowni* occur throughout the soil profile with cross-cutting relationships showing continuing occupation through changing environmental conditions, with the greatest concentration in the Bkb horizon with an average bioturbation percentage of 40.9, recording a greater response of the tracemaking organisms to environmental conditions during this time. Invertebrate activity was identified to be highly localized (diffusive mixing) and does not greatly affect the sequence of reconstructed vegetation assemblages, particle size distribution, or soil color unless material is being moved across a distinctive horizon boundary. Therefore, the 5 cm sampling interval used at the Old Wauneta Roadcut site is an adequate strategy to account for biota activity at this location.

1. Introduction

Continental bioturbation is a process of sediment mixing created by the feeding and burrowing of invertebrates, vertebrates, and growth of root systems (e.g., Hasiotis, 2003, 2007; Hole, 1981; Thorp, 1949). These behaviors result in traces (i.e., krotovina or crotovina) that are studied through the discipline of ichnology. Additions of organic

material by flora and fauna, along with their ability to mix sediment and produce soil peds, can create an organically rich, well-structured soil through time. Bioturbation, however, can have negative consequences on research directed at reconstructing climate variables from paleosols (e.g., Grave and Kealhofer, 1999; Stein, 1983). Mixing of sediment during and following soil formation may create discrepancies in age determinations and proxy analyses, such as stable carbon isotope, organic carbon, or grain-size distributions.

The purpose of this research is to evaluate the degree of bioturbation in the formation of the Brady Soil in southwestern Nebraska that marks the Pleistocene—Holocene transition (PHT). The objectives of this study are to (1) assess the morphology and scale of disturbance within the paleosol due to floral and faunal bioturbation and (2) evaluate its effects on paleoenvironmental proxy data and age constraints. Brady Soil pedogenesis occurred at a time of rapid climate change during the final stages of deglaciation in the Northern Hemisphere. This paleosol is an important source of climate proxy data for the North American continental interior and has been the focus of paleoenvironmental reconstructions in recent years (Jacobs and Mason, 2004; Mason et al., 2008; Miao et al., 2007; Woodburn et al., n.d.). These previous studies have noted bioturbation in the Brady Soil throughout the central Great Plains, nevertheless, sampling strategies and proxy validity in reference to sediment mixing has not been fully considered. In this study, we describe the stratigraphy, trace morphology, micromorphological characteristics of sediments, and distribution of phytolith assemblages in the Peoria Loess, Brady Soil, and Bignell Loess to estimate the extent of mixing within the soil profile.

2. Background

2.1. Assessing bioturbation in continental settings

The role of bioturbation in soil formation is relatively well known and discussed in the fields of pedology, geology, and paleontology. In the field of ichnology (study of floral and faunal behavior and traces), trace fossils are used in particular for paleobiological and paleoenvironmental reconstructions (e.g., Bromley, 1996; Ekdale et al., 1984; Hasiotis, 2003, 2007; Hole, 1981; Thorp, 1949). Ichnological research has classically focused on marine environments, and to a lesser degree on the continental realm. Research specifically in aeolian environments has been concentrated on modern and ancient sand-dominated deposits (e.g., Ahlbrandt et al., 1978; Ekdale et al., 2007; Hasiotis, 2002; Radies et al., 2005; Schmeisser et al., 2009), whereas little research has been conducted on bioturbation in loess deposits (e.g., Jacobs and Mason, 2004; Tobin, 2004a; Tobin, 2004b).

Interpretations of floral and faunal behavior, aeolian depositional history, fluctuations of soil moisture and water tables, and changes in climate are made by comparing modern bioturbation with trace fossil equivalents (e.g., Hasiotis, 2002; Parrish, 1999; Smith and Hasiotis, 2008; Counts and Hasiotis, 2009; Smith et al., 2009). While bioturbation is extensively noted in literature as a characteristic of a soil (e.g., Kemp et al., 2001; Kemp et al., 2003; Mason et al., 2007; Pye, 1995), the environmental interpretations have not been made, and its influence as a source of error in dating techniques and proxy accuracy is frequently overlooked.

Studies have successfully shown that the analysis of bioturbation is key to understanding event sequences or archaeological artifact location within a soil. Grave and Kealhofer (1999) were able to determine the extent of artifact movement using burrow and fill characteristics along with bounding soil ages, soil macro- and micromorphology, and phytolith analyses. Related studies by Stein (1983), Lim et al.

(2007), and Van Nest (2002) demonstrated the importance of defining local (diffusive) versus non-local (advective) mixing when looking at disruption of proxy indicators and assessing accuracy of data. Additionally, investigators have promoted the use of distinctive burrow layers as defining characteristics and time markers for stratigraphic units across regional geographic extents (Lim et al., 2007; Tobin, 2004a), as well as being important paleoenvironmental indicators (Jacobs and Mason, 2004; Smith et al., 2008; Counts and Hasiotis, 2009).

2.2. Micromorphology

Micromorphology allows for the study of soil features and fabrics at the microscopic scale and provides useful information to reconstruct environmental processes that drove soil formation and alteration (e.g., Grave and Kealhofer, 1999; Gunal and Ransom, 2006; Kemp, 1999; Kemp, 2007; Kemp et al., 2001; Stoops, 2003). Soil features produced by faunal and floral activity are differentiated from features produced by pedologic processes through the identification and classification of granular and spongy microstructures indicative of excrement, calcitic biospheroids, infilling, meniscate backfilling, channel microstructures, and well-oriented clay coatings (e.g., Driese et al., 2005, 2008; Kemp, 2007; Kemp et al., 2003; Smith et al., 2008; Stoops, 2003). Location of structures and sediment within the soil profile provides a timeline for events of bioturbation and soil formation—depth of faunal and floral structures depicts either episodes of accretion with bioturbation occurring simultaneously, or instances of bioturbation occurring post-deposition (Halfen and Hasiotis, 2010; Hasiotis, 2007; Hasiotis, 2002; Kemp et al., 2003).

2.3. Phytolith Analysis

Vegetation assemblage variations within a soil or sediment profile can be used to track isolated sediment movements (Grave and Kealhofer, 1999), particularly if assemblages are fairly distinctive and transition through time. Paleovegetation analysis

was accomplished herein using phytoliths. Opal phytoliths are microscopic silica bodies formed by the uptake of water and dissolved minerals from the soil and subsequent precipitation of silica within plant cells (Mulholland and Rapp Jr., 1992b; Piperno, 1988; Piperno, 2006). Most phytoliths are silica casts of specific plant cells and can be classified at various taxonomic levels. Shortcell phytoliths in grasses can be identified to subfamily and, occasionally, even genus level (Piperno, 2006). Opal phytolith analysis is used to quantify paleovegetation assemblages of grass subfamilies (Pooideae, Chloridoideae, and Panicoideae) and other diagnostic phytoliths, including those of trees and shrubs. Diagnostic grass shortcells consist of shapes described as bilobate, cross, saddle, and trapezoid—each with many variations (Brown, 1984; Mulholland and Rapp Jr., 1992a). Distinguishable dicotyledon (trees and shrubs) phytoliths include spheres, polyhedrons, jigsaw-puzzle pieces, honeycomb assemblages, branched tracheids, segmented hairs, scalloped phytoliths, and platelets (Bozarth, 1992; Wilding and Drees, 1973).

Such soil microfossils as phytoliths and other biosilicates present an optimal resource for paleoenvironmental reconstructions in the Great Plains where grasses dominate and archives of fossil pollen grain records are rare due to the paucity of natural lakes. Phytolith formation occurs in most plants and remains in soil sediment after source plant material decays. Preservation of biosilica, however, depends on physical and chemical factors of the soil environment, and fortuitously, the Great Plains is well suited for phytolith preservation due to relatively high pH levels within sediment and soil (Fredlund et al., 1985; Piperno, 2006). Nevertheless, dicotyledon phytoliths are underrepresented due to low production of silica bodies in trees and shrubs and to poor preservation of the thin, fragile polyhedral-type phytoliths produced (Piperno, 2006).

3. Study Site

The Old Wauneta Roadcut (40.500561° N, 101.417872° W; ~1017 m amsl) is located 10 km northwest of the town of Wauneta in Chase County, Nebraska and occurs along the Sand Hills-loess transition (Fig. 1). This abandoned roadcut sits on a topographical high on the northern edge of a loess-mantled upland with the broad valley of Spring Creek to the north. It is a west-facing, vertical cut that exposes late-Quaternary stratigraphy including the late-Wisconsinan Peoria Loess and Holocene Bignell Loess separated by the Brady Soil that formed during the PHT between ~14.7 to 9 cal ka (Baars and Maples, 1998; Mason et al., 2008). This location provides a well-developed, ~1-m-thick exposure of the Brady Soil, which is highly bioturbated, and has detailed paleoenvironmental proxy records and age constraints reported by previous investigators (Jacobs and Mason, 2004; Mason et al., 2008; Miao et al., 2005; Woodburn et al., n.d.).

Modern climate characteristics, recorded at Wauneta, NE, include a January mean temperature of -1.3°C, a July mean temperature of 25.7°C, and mean annual precipitation of 493 mm with the majority of the precipitation occurring in summer months (HPRCC, 2013). Vegetative cover consists of a mixed-grass prairie with a variety of forbs. Climate conditions during the time of Brady Soil formation ranged from cool, mesic conditions in the late Pleistocene to warmer and more arid environment in the early Holocene (Cordova et al., 2011; Mason et al., 2008; Miao et al., 2007).

4. Methods

Soil macromorphology of the Old Wauneta Roadcut site was described in the field following the National Soil Survey Center's *Field Book for Describing and Sampling Soils* (Schoenberger et al., 2002), and using the Munsell Soil Color Chart (1992) for color designations. Profile sketches and digital images taken of large- and small-scale features accompanied on-site descriptions. Bioturbation was documented by

sediment excavation, counting, and measuring trace fossil diameters and length, width, and height of larger chambers. Quantifying type and size of burrows established biota diversity and bioturbation intensities, which were correlated to local versus non-local mixing events. Architecture and morphologies of burrows and root traces were described in the field for preliminary interpretations, and extensive photographs of bioturbation evidence were taken for analysis. Additionally, eight sediment samples were taken from burrow fill throughout the profile for further analysis.

The approach for quantifying bioturbation percentage was adapted from the intersection grid method for bedding plane surfaces as described by Marenco and Bottjer (2010). In this study, digital images of thin section samples were used instead of images of bedding planes. A digital grid was overlain on the images with a frame of ~300 mm^2 (~15 x 20 mm^2). Grids were marked at every intersection that touched a trace on the digital images. Given the inconsistent coverage of sediment on a thin section slide, the grid intersections that touched empty space related to a thinning of sediment or empty space of unknown origin was removed from the total area of the grid, as well as those that meet empty root traces. Intersections along the outer grid frame were excluded from analysis (Marenco and Bottjer, 2010). Intersection points touching filled traces were marked, counted and divided by the total number of grid intersections for the slide to calculate percent of the thin section that is bioturbated. Percentages of bioturbation from thin sections were compared to semi-quantification designations for the soil profile using the bioturbation index (Taylor and Goldring, 1993), utilizing profile images and field observations. The bioturbation index employs descriptive terms to define degree of bioturbation based on trace density, trace overlap, and bedding boundary sharpness, and relates descriptions to an estimated bioturbation percentage. As defined by Taylor and Goldring (1993), the index delineates six grades: BI 0 (no traces), BI 1 (1-4% sparse traces with distinct bedding), BI 2 (5-30% low trace density with distinct bedding), BI 3

(31-60% moderate trace density with rare overlap and sharp bedding boundaries), BI 4 (61-90% high trace density with common overlap and indistinct bedding), BI 5 (91-99% intense bioturbation with limited reworking and bedding barely intact), and BI 6 (complete bioturbation).

Assessing micromorphology entailed thin section production of block samples from horizons within the soil profile, loess sediments, and burrow fills. All samples obtained did not remain intact through thin section production process, however, thin sections for the Bignell Loess, Brady Ab, ABb, and Bkb horizons were successfully processed, together with ten burrow samples – eight of which have corresponding phytolith, L*a*b color, and particle size data. Sampling procedures followed those of Murphy (1986) and Josephs and Bettis (2003), insuring that orientation of sediment blocks removed were marked as to original depth and orientation in the profile. Preparation of thin-section slides from block samples was completed at the University of Kansas Geology Department and by Texas Petrographic Services Inc. Analysis to ascertain micromorphologic characteristics of faunal and floral traces was completed according to Stoops (2003), using a polarizing microscope with a Nikon camera system.

To provide high-resolution data for the soil profile, twenty-eight consecutive samples ~5cm high x 3cm wide x 3cm deep were taken starting in the lowermost portion of the Bignell Loess, through the Brady Soil, and ending in the uppermost portion of the Peoria Loess. Laboratory analyses for L*a*b color, particle size distribution, and phytolith assemblages were performed on the profile samples as well as eight samples from burrow fill. L*a*b color parameters are used here to quantitatively differentiate subtle variations in soil colors that could not be detected using the Munsell color chart. Measured by the Konica Minolta Spectrophotometer, color indices are separated into luminance or lightness (L) with values ranging from 0 for black to 100 for white, and chromatic values for redness (a; positive values are more red, negative are more green)

and yellowness (b; positive values are more yellow, negative are blue). All color designations reported are for moist soil. Summarized particle size data was obtained using a Malvern Mastersizer 2000 laser diffraction particle size analyzer following a 3-minute sonication in deionized water.

Phytoliths and other biosilicates were extracted from 5 g of sediment after dissolution of carbonates using 10% HCL, clay removal with sodium pyrophosphate, and oxidation of organic matter using 30% H_2O_2 and heated in a hot water bath until reaction subsided (Bozarth, 2008). Separation of biosilicates from most other mineral matter was accomplished using a $ZnBr_2$ (d = 2.3) heavy liquid floatation (Bozarth, 2008). Samples were mounted on microscope slides in immersion oil to allow for 3D observation. Transects were scanned until ≥200 shortcell phytoliths were counted and identified according to Twiss et al. (1969), Brown (1984), Bozarth (1992), and Wilding and Drees (1973). Additional biosilicates, such as large cell phytoliths, sponge spicules, algal statosphores, and diatoms, were tallied during microscopic analysis as supplementary proxy data. Frequency records have been rendered in graphical format using the Tilia program (Grimm, 2011) with assemblages displayed as percentages of the sum of shortcell phytoliths.

5. Results

5.1. Macromorphology

The surface of the Brady Soil Ab horizon, indicated by a very dark gray soil color (~10YR 3/1), begins ~580 cm below the modern surface at the sampled profile (Figs. 2, 3). Though above this is an ACb horizon, which reveals soil formation being extinguished by the start of Bignell loess deposition. This period of increasing dust influx is signified by a lightening in color to a dark grayish brown (10YR 4/2) in the

ACb, which continues into the Bignell Loess to grayish brown (~10YR 5/2). The Ab horizon transitions into an ABb horizon that remains similarly dark in color (~10YR 4/1), but displays a slight pick-up in carbonate content. A continued pick-up in illuvial clay and carbonate content occurs at the base of the solum in the Bkb horizon, which displays a lighter brown color (~10YR 4/3), similar to that of the Peoria Loess. The transition of color from the top of the Bkb horizon into the Peoria Loess is not distinguishable using the Munsell color chart so the boundary between the loess and Bkb soil horizon could not characterized in the field. Field texture classification was silt loam for the entire profile, which also impeded designations of horizon boundaries. L*a*b color and particle size distribution were useful in differentiating the Bkb/Peoria Loess boundary (Fig. 8).

Considerable bioturbation by plant roots, invertebrates, and small vertebrates is found within the Brady Soil and bounding loess units (Figs. 2-8). Bioturbation was not restricted to a single period of pedogenesis, but occurred continually through time, represented by differing sediment fills and crosscutting relationships (Figs. 2, 4). Large chamber (~30cm high x 40cm long) and burrow (~6 to 12 cm wide) systems throughout the soil profile (Figs. 2, 4), and architecture displayed by open burrows (Fig. 5), suggest that a rodent, such as a prairie dog (*Cynomys* sp.) or ground squirrel (*Spermophilus* sp.), is responsible for their production (Sheets et al., 1971; Tobin, 2004b). The Bkb horizon, however, is dominated by extensive, small (~2 cm width), backfilled burrows with distinctive menisci (Figs. 2, 6), assigned to the ichnotaxon *Naktodemasis bowni* and typically produced by cicada nymphs (Cicadae), burrower bugs (Cydnidae) or possibly ground beetles (Carabidae) and scarab beetles (Scarabaeidae) (Smith et al., 2008; Counts and Hasiotis, 2009). Numerous indicators for floral bioturbation were seen in the form of small, decayed roots and rhizoliths. Many were backfilled, but thin section analysis

exposed many with partial backfill and even unfilled with secondary and tertiary branching still intact (Fig. 8).

Percentage of bioturbation (not including empty root traces) estimated by the intersection grid method on thin section slides (Fig. 7) shows that even within the loess fill of rodent burrows, the trace density is at 17.3%. Percentages are an estimate and vary depending on location within a horizon, however where multiple thin sections were available, an average value was calculated. Traces within the standard soil profile occur in greater concentrations and percentages are as follow: Bignell Loess 26.4%, Brady Ab horizon 50.7%, Brady ABb horizon averaged 41% (33.7% and 48.3%), Brady Bkb horizon averaged 40.9% (from 36.2%, 44.8%, and 41.6%) (Fig. 7). The intersection grid method does not take into account the amount of overlap in respect to trace quantification and, with the use of thin sections, does not provide a clear, overall estimation of activity. To counter these limitations, the semi-quantitative bioturbation index was used to evaluate the soil profile. Based on descriptions provided by Taylor and Goldring (1993), the Bignell Loess would fall within the BI 2 class that has the same general percent bioturbation (5-30%) as seen with the thin section sample. However, the Brady Ab, ABb, and Bkb horizons have a larger estimated percent bioturbation (61-90%) than the intersection grid method indicated due to overlap of traces. The Brady Ab and ABb horizons are designated BI 4 due to the numerous, large rodent chambers and burrows with common overlap (Fig. 4). The high density and common overlap of *N. bowni* burrows within the Brady Bkb horizon, along with indistinct horizon boundary puts this horizon into the BI 4 category as well (Fig. 6).

5.3. Micromorphology

Samples for thin section production in the loess and soil horizon matrix were oriented vertically and taken in locations that appeared to be relatively undisturbed. Once in thin section format, however, these samples proved to be highly bioturbated, showing

floral ped features such as rhizoliths and pore spaces from primary and secondary root systems, and faunal traces of small burrows with locally-derived fill, and earthworm excrement, similar in color to the matrix material (Figs. 2, 3). These burrows are typically similar or smaller in size to those produced by cicada nymphs. The two samples from Ab and ABb horizon material also have open pores indicative of earthworm burrows and root cavities that have remained unfilled. As the Bkb horizon thin section reveals, locating a relatively undisturbed block sample was problematic due to the prevalence of *N. bowni* burrows (Figs. 2, 3). Thin sections taken within the large rodent burrows consist of sediment that is primarily non-local infill, but also contain smaller traces from burrowing that occurred after the infill was in place (Fig.8).

*5.3. Particle size distribution and L*a*b color variations*

The Brady Soil and bounding loess units are dominated by silt-sized particles (2-63 μm) with an average of 55% in the Bignell Loess, increasing to between 60 and 70% through the soil horizons, with just a slight decrease in the Peoria Loess. Sand (>63 μm) percents increase during times of heavier loess influx indicating periods of slightly stronger winds. Low quantities of clay-sized particles (<2 μm) are found within the profile, averaging 3% throughout (Fig. 9). L*a*b color parameters show a much greater variation within horizon material than visually indicated. The Ab and ABb horizons do have very similar coloring and are darker values, however, the individual points of lighter coloring in the Ab horizon is most likely a product of bioturbation. The bounding loess units shift to lighter coloring with increasing red and yellow hues. Within the Bignell Loess, the color darkens once again, however, field Munsell coloring does not detect this shift (Fig. 9).

The eight burrow fill samples are compared to the particle size and color parameters for the soil profile in Fig. 8. *N. bowni* traces were sampled within the Bignell Loess unit (burrow 9) and the upper Bkb soil horizon (burrow 5). Burrow 9 is very

similar in composition and color to the surrounding matrix indicating localized mixing within this zone. Burrow 5 is similar to particle size and color values found just above in the ABb horizon, also representing localized mixing. Burrows 1, 2, 3, and 4 are larger rodent burrows within the Ab horizon along with the large chamber. All show similar patterns with more sand and less silt than the surrounding soil matrix along with increased red and yellow parameters similar to that of the Bignell Loess, correlating to non-local, deep mixing events. The darkening seen in burrows 2, 3, and 4 is due to further mixing of the fill sediment by later localized bioturbation as seen in the thin sections (Fig. 8). Burrow 8, within the Peoria Loess, has very similar particle size composition to that of the A horizon, as well as chromatic characteristics of surrounding loess material, however, luminance values are even lower than those found in A horizons (Fig. 9). Fill sediment from burrow 8 is similar to burrows 2, 3, and 4, and contains a mix of distinct dark colored soil matrix and light colored loess material due to additional bioturbation after infill occurred.

5.4. Phytolith analysis

Vegetation assemblages from relatively undisturbed soil and loess sediment show a well-defined pattern of transition through the Brady Soil (Fig. 10). During the onset of Brady Soil formation cool, mesic conditions produced a savannah to open woodland setting signified by the peak in tree and shrub phytolith types such as spheres, polyhedral, elongate honeycomb, and jigsaw puzzle piece-types, and dominance of Pooideae cool-season grasses. Vegetation changes are seen at a depth of ~630 to 610 cmbs where a decrease in trees and shrubs and a distinct occurrence of *Stipa*-type phytoliths indicates the shift to an open grassland environment. *Stipa* is a genus-level Pooideae grass that is adapted to dry environments, marking the transition from cool, mesic conditions in the late Pleistocene to the warm, arid conditions in the early Holocene. Early-Holocene mixed-grass prairies are found above 610 cmbs, with almost equal quantities of cool-

season Pooideae and warm-season Chloridoideae grasses. In addition, biosilicates such as diatoms and sponge spicules occur with increased concentrations during times of greater loess sediment influx in the Peoria Loess, lower zones of Brady Soil formation, and Bignell Loess units.

Phytolith analysis of the eight burrows and chamber samples (Fig. 11) show similar quantities of Pooideae and Chloridoideae grasses throughout, yet, slightly greater Chloridoideae values do occur in burrows within the upper Ab horizon and Bignell Loess. Chloridoideae quantities in all burrow fills, except burrow 2, are greater than in adjacent soil matrix showing a downward dispersion through burrow systems. This is corroborated by frequencies of diatoms, sponge spicules, and algal statosphores in the chamber and in burrows 1, 3, and 4, which indicate downward movement of loess material. Lack of distinctive *Stipa*-type phytoliths in the samples between ~630 to 610 cmbs implies localized mixing in this zone is not a major contribution to the bioturbation signal within the burrow sediments. Burrow 2 has a different sediment source than the other burrows in this zone; it shows similar frequencies of Chloridoideae and Pooideae grasses as those in adjacent soil and a large peak in phytolith concentration similar to that produced in the upper portion of the Ab horizon. In addition, burrow 8, occurring at 685 cmbs, has a similar peak in concentrations signifying a large input of sediment from the Ab horizon. Phytolith assemblages from *N. bowni* traces (burrows 9 and 5), correlate to local vegetation compositions found just a few centimeters above sample locations. AMS radiocarbon dating of an *N. bowni* trace in the Bkb horizon (near burrow 5) provided an age of 11,250 +/- 50 ^{14}C yrs BP (13,085 +/- 57 calib yrs BP; Fairbanks, 2005). Age comparison with those from the soil profile (Mason et al., 2008; Fig.3) substantiates sediment movement from the lower ABb horizon into the upper Bkb.

6. Discussion

Macro- and micromorphologic data have shown extensive evidence for invertebrate and vertebrate activity (BI 4 in the Brady Ab, ABb, and Bkb horizons). Brady Soil tracemakers have been determined based on comparisons with modern analogs of burrowing organisms and their structures produced, as well as other late Pleistocene burrows with similar size and architecture, in which, biota remains were found. *N. bowni* ichnotaxon found within the Brady Soil profile are produced by cicada nymphs (Cicadidae) or burrower bugs (Cydnidae). These invertebrates produce distinctive meniscate backfills with nested, discrete, ellipsoidal packets (Figs. 2, 6; Smith and Hasiotis, 2008; Smith et al., 2008; Counts and Hasiotis, 2009). Thin section analysis provided evidence for earthworm traces (*Edaphichnium*) including reproductive cocoons and granular and spongy microstructures indicative of excrement (Hasiotis, 2002; Stoops, 2003), as well as decayed roots with no to complete back filling, and rhizoliths with secondary and tertiary branching still intact and unfilled within sediment (Fig. 8). Large burrow and chamber dwellings (domichnia) were constructed by prairie dog (*Cynomys* sp.) or ground squirrel (*Spermophilus* sp.) as evidenced by the size and architecture of the domichnia and scratch marks noted in unfilled tunnels (Figs. 2, 4, 5; Sheets et al., 1971; Tobin, 2004a, 2004b). Based on particle size, L*a*b color, and phytolith signals, rodent burrows are sources of non-local (advective) mixing with infill from upper profile units, specifically from Bignell Loess (as fill within burrows 1, 3, 4, and the chamber) and from Ab horizon soil (as fill within burrows 2, and 8). Instances of burrow systems containing passive fill (infill from surface sediments falling into open burrows and chambers) of lighter-colored loess sediment represent post-soil formation bioturbation events (Figs. 2, 4). In addition, cross-cutting relationships and fill made of dark soil material suggests bioturbation events taking place during pedogenesis (Figs. 2, 4), indicating long-term

activity by rodent populations. Similarly, cicada nymph or burrower bug traces occur throughout the soil profile with cross-cutting relationships showing continuing occupation through changing environmental conditions. The greatest concentration of *N. bowni* ichnofossils, however, is in the Bkb horizon with an average bioturbation percentage of 40.9, recording a greater response of the tracemaking organisms to environmental conditions during this time.

Through integration of large- and small-scale analyses, invertebrate activity was identified to be highly localized (diffusive mixing) to an average of ~5 cm and does not greatly affect the sequence of reconstructed vegetation assemblages, particle size distribution, or soil color unless material is being moved across a distinctive horizon boundary. Large rodent domichnia has a greater impact on proxy redistribution through the removal of material and subsequent infill of sediments from above, creating deep, non-local mixing patterns. Yet, invertebrate activity within the non-local burrow fill facilitates slight normalization of sediment characteristics with those of the adjacent matrix. These large burrows are typically easy to detect within the surrounding soil matrix due to color changes and loose consistency of the fill compared to *in situ* matrix material and can be avoided during profile sampling.

7. Conclusions

Sampling strategies for proxy reconstructions and age determinations should be selected with respect to bioturbation patterns observed within a given profile. Additionally, resolution should be appropriate for the occurrence of less visible, local (diffusive) mixing. Based on multiple proxy analyses included in this and previous studies of the Brady Soil (Miao et al., 2007; Woodburn et al., in review), a relatively high-resolution environmental reconstruction can be produced reliably with a 5-cm

sampling increment. This resolution makes allowances for pedogenic features that are integrated by local mixing events without losing desired detail. Sampling strategies of 2-cm increments recorded for the same location (Miao et al., 2007) show similar proxy trends, but with much more variability likely attributable to mixing events. Age constraints provided by Mason et al. (2008) (Fig. 3), Miao (2007), and Johnson and Willey (2000) further verify stratigraphic integrity through sediment with localized invertebrate mixing.

Additionally, bioturbation provides valuable information to paleoenvironmental reconstructions in reference to faunal presence and associated environmental conditions in which they live. For the Brady Soil profile, specifically, the presence of *Naktodemasis bowni* indicates tracemakers such as cicada nymphs (Cicadidae) and burrower bugs (Cydnidea). Modern cicada nymph burrows tend to be correlated to the presence of woody vegetation needed throughout the cicada's life cycle (O'Geen and Busacca, 2001). Cicada nymphs feed on tree and shrub root sap, while adults lay eggs on and use the rough bark of aboveground woody vegetation to assist in exoskeleton molting (Jacobs and Mason, 2004; O'Geen and Busacca, 2001). Increased activity of cicada within the Bkb horizon corroborates phytolith reconstruction, indicating savannah to open woodland conditions during this time of Brady Soil pedogenesis (Woodburn et al., in review).

Acknowledgements

Financial support for this work was provided by the University of Kansas General Research Fund and Kollmorgen Fellowship Award from the University of Kansas Department of Geography. We are grateful to the landowners for their cooperation in allowing us to collect soil samples at the old roadcut site. We also

acknowledge Wayne Dickerson in the University of Kansas Geology Department for thin-section production.

References

Ahlbrandt, T.S., Andrews, S. and Gwynne, D.T., 1978. Bioturbation in eolian deposits. Journal of Sedimentary Research, 48(3): 839-848.

Baars, D.L. and Maples, C.G. (Editors), 1998. Lexicon of Geologic Names of Kansas (through 1995), Bulletin 231. Kansas Geological Survey, Lawrence, KS.

Bozarth, S.R., 1992. Classification of opal phytoliths formed in selected dicotyledons native to the Great Plains. In: G. Rapp Jr. and S.C. Mulholland (Editors), Phytolith Systematics: Emerging Issues. Plenum Press, New York, pp. 193-214.

Bozarth, S.R., 2008. Procedure for Extraction of Opal Phytoliths from Sediment, unpublished manuscript.

Bromley, R., 1996. Trace fossils: biology, taphonomy and applications. Psychology Press.

Brown, D.A., 1984. Prospects and limits of a phytolith key for grasses in the central United States. Journal of Archaeological Science, 11: 345-368.

Cordova, C.E., Johnson, W.C., Mandel, R.D. and Palmer, M.W., 2011. Late Quaternary environmental change inferred from phytoliths and other soil-related proxies: Case studies from the central and southern Great Plains, USA. Catena, 85: 87-108.

Counts, J.W. and Hasiotis, S.T., 2009. Neoichnological experiments with masked chafer beetles (Coleoptera: Scarabaeidae): implications for backfilled continental trace fossils. PALAIOS, 24(2): 74-91.

Driese, S.G., Nordt, L.C., Lynn, W.C., Stiles, C.A., Mora, C.I., and Wilding, L.P., 2005. Distinguishing Climate in the Soil Record Using Chemical Trends in a Vertisol Climosequence from the Texas Coast Prairie, and Application to Interpreting Paleozoic Paleosols in the Appalachian Basin, U.S.A. Journal of Sedimentary Research, 75(3): 339-349.

Driese, S., Li, Z. and McKay, L., 2008. Evidence for multiple, episodic, mid-Holocene Hypsithermal recorded in two soil profiles along an alluvial floodplain catena, southeastern Tennessee, USA. Quaternary Research, 69(2): 276-291.

Ekdale, A.A., Bromley, R.G. and Loope, D.B., 2007. Ichnofacies of an ancient erg: a climatically influenced trace fossil association in the Jurassic Navajo Sandstone, southern Utah, U.S.A. In: W. Miller III (Editor), Trace Fossils: Concepts, Problems, Prospects. Elsevier, Amsterdam, pp. 562-574.

Ekdale, A.A., Bromley, R.G. and Pemberton, S.G., 1984. Ichnology: the use of trace fossils in sedimentology and stratigraphy. SEPM Short Course, 15, 317 pp.

Fairbanks, R.G., Mortlock, R.A., Chiu, T., Cao, L., Kaplan, A., Guilderson, T.P., Fairbanks, T.W., Bloom, A.L., Grootes, P.M., and Nadeau, M., 2005. Radiocarbon calibration curve spanning 0 to 50,000 years BP based on paired $^{230}Th/^{234}U/^{238}U$ and ^{14}C dates on pristine corals. Quaternary Science Reviews, 24: 1781-1796.

Fredlund, G.G., Johnson, W.C. and Dort Jr., W., 1985. A Preliminary Analysis of Opal Phytoliths from the Eustis Ash Pit, Frontier County, Nebraska. Institute for Tertiary-Quaternary Studies - TER-QUA Symposium Series(1): 147-162.

Grave, P. and Kealhofer, L., 1999. Assessing bioturbation in archaeological sediments using soil morphology and phytolith analysis. Journal of Archaeological Science, 26(10): 1239-1248.

Grimm, E.C., 2011. Tilia. Illinois State Museum Research and Collections Center, Springfield, IL.

Gunal, H. and Ransom, M., 2006. Clay illuviation and calcium carbonate accumulation along a precipitation gradient in Kansas. Catena, 68(1): 59-69.

Halfen, A.F. and Hasiotis, S.T., 2010. Neoichnological study of the traces and burrowing behaviors of the western harvester ant *Pogonomyrmex occidentalis* (Insecta: Hymenoptera: Formicidae): paleopedogenic and paleoecological implications. PALAIOS, 25(11): 703-720.

Hasiotis, S., 2007. Continental ichnology: fundamental processes and controls on trace fossil distribution. Trace Fossils: Concepts, Problems, Prospects: Elsevier, Amsterdam: 262–278.

Hasiotis, S.T., 2002. Continental Trace Fossils. SEPM Short Course Notes, 51, Tulsa, Oklahoma, 134 pp.

Hasiotis, S.T., 2003. Complex ichnofossils of solitary and social soil organisms: understanding their evolution and roles in terrestrial paleoecosystems. Palaeogeography, Palaeoclimatology, Palaeoecology, 192(1-4): 259-320.

Hole, F.D., 1981. Effects of animals on soil. Geoderma, 25(1-2): 75-112.

HPRCC, 2013. Historical Data Summaries. High Plains Regional Climate Center http://www.hprcc.unl.edu/data/historical/.

Jacobs, P.M. and Mason, J.A., 2004. Paleopedology of soils in thick Holocene loess, Nebraska, USA. Revista Mexicana de Ciencias Geologicas, 21(1): 54-70.

Johnson, W.C. and Willey, K.L., 2000. Isotopic and rock magnetic expression of environmental change at the Pleistocene-Holocene transition in the central Great Plains. Quaternary International(67): 89-106.

Josephs, R.L. and Bettis, E.A., 2003. Short contribution: A practical alternative to Kubiena boxes for the collection of samples for micromorphological analysis. Geoarchaeology-an International Journal, 18(5): 567-570.

Kemp, R.A., 1999. Micromorphology of loess-paleosol sequences: a record of paleoenvironmental change. Catena, 35(2-4): 179-196.

Kemp, R.A., 2007. Paleosols and wind-blown sediments | Soil Micromorphology. In: A.E. Editor-in-Chief: Scott (Editor), Encyclopedia of Quaternary Science. Elsevier, Oxford, pp. 2103-2114.

Kemp, R.A., Derbyshire, E. and Meng, X.M., 2001. A high-resolution micromorphological record of changing landscapes and climates on the western Loess Plateau of China during oxygen isotope stage 5. Palaeogeography Palaeoclimatology Palaeoecology, 170(1-2): 157-169.

Kemp, R.A., Toms, P.S., Sayago, J.M., Derbyshire, E., King, M., and Wagoner, L., 2003. Micromorphology and OSL dating of the basal part of the loess-paleosol sequence at La Mesada in Tucuman province, Northwest Argentina. Quaternary International, 106: 111-117.

Lim, H.S., Lee, Y., Yi, S., Kim, C., Chung, C., Lee, H., and Choi, J.H., 2007. Vertebrate burrows in late Pleistocene paleosols at Korean Palaeolithic sites and their significance as a stratigraphic marker. Quaternary Research, 68(2): 213-219.

Marenco, K.N., and Bottjer, D.J., 2010. The intersection grid technique for quantifying the extent of bioturbation on bedding planes. PALAIOS, 25: 457-462.

Mason, J.A., Joeckel, R.M. and Bettis III, E.A., 2007. Middle to Late Pleistocene loess record in eastern Nebraska, USA, and implications for the unique nature of Oxygen Isotope Stage 2. Quaternary Science Review, 26(5-6): 773-792.

Mason, J.A., Miao, X., Hanson, P.R., Johnson, W.C., Jacobs, P.M., and Goble, R.J., 2008. Loess record of the Pleistocene-Holocene transition on the northern and central Great Plains, USA. Quaternary Science Review, 27: 1772-1783.

Miao, X., Mason, J.A., Goble, R.J. and Hanson, P.R., 2005. Loess record of dry climate and aeolian activity in the early- to mid-Holocene, central Great Plains, North America. The Holocene, 15(3): 339-346.

Miao, X., Mason, J.A., Johnson, W.C. and Wand, H., 2007. High-resolution proxy record of Holocene climate from a loess section in Southwestern Nebraska, USA. Palaeogeography, Palaeoclimatology, Palaeoecology(245): 368-381.

Mulholland, S.C. and Rapp Jr., G., 1992a. A Morphological Classification of Grass Silica-Bodies. In: G. Rapp Jr. and S.C. Mulholland (Editors), Phytolith Systematics: Emerging Issues. Plenum Press, New York, pp. 65-90.

Mulholland, S.C. and Rapp Jr., G., 1992b. Phytolith Systematics: An Introduction. In: G. Rapp Jr. and S.C. Mulholland (Editors), Phytolith Systematics: Emerging Issues. Plenum Press, New York, pp. 1-13.

Munsell Color, 1992. Munsell Soil Color Charts. Revised Edition. Macbeth, Division of Kollmorgen Instruments Corp. Newburgh, New York.

Murphy, C.P., 1986. Thin Section Preparation of Soils and Sediments. A B Academic Publishers, Berkhamsted, Great Britain, 149 pp.

O'Geen, A.T. and Busacca, A.J., 2001. Faunal burrows as indicators of paleo-vegetation in eastern Washington, USA. Palaeogeography, Palaeoclimatology, Palaeoecology, 169(1–2): 23-37.

Parrish, J.T., 1999. Interpreting Pre-Quaternary Climate from the Geologic Record. Columbia University Press, New York, 354 pp.

Piperno, D.R., 1988. Phytolith Analysis: An Archaeological and Geological Perspective. Academic Press, Inc., San Diego.

Piperno, D.R., 2006. Phytoliths: A Comprehensive Guide for Archaeologists and Paleoecologists. AltaMira Press, Lanham, MD, 238 pp.

Pye, K., 1995. The nature, origin and accumulation of loess. Quaternary Science Reviews, 14(7-8): 653-667.

Radies, D., Hasiotis, S., Preusser, F., Neubert, E. and Matter, A., 2005. Paleoclimatic significance of Early Holocene faunal assemblages in wet interdune deposits of the Wahiba Sand Sea, Sultanate of Oman. Journal of Arid Environments, 62(1): 109-125.

Schmeisser, R., Loope, D. and Wedin, D., 2009. Clues to the Medieval destabilization of the Nebraska Sand Hills, USA, from ancient pocket gopher burrows. PALAIOS, 24(12): 809.

Schoenberger, P.J., Wysocki, D.A., Benham, E.C. and Broderson, W.D. (Editors), 2002. Field Book for Describing and Sampling Soils, Version 2.0. Natural Resources Conservation Service, National Soil Survey Center, Lincoln, NE.

Sheets, R.G., Linder, R.L. and Dahlgren, R.B., 1971. Burrow Systems of Prairie Dogs in South Dakota. Journal of Mammalogy, 52(2): 451-453.

Smith, J.J. and Hasiotis, S.T., 2008. Traces and burrowing behaviors of the cicada nymph *Cicadetta calliope*: Neoichnology and paleoecological significance of extant soil-dwelling insects. PALAIOS, 23(8): 503-513.

Smith, J.J., Hasiotis, S.T., Kraus, M.J. and Woody, D.T., 2008. *Naktodemasis bowni:* New ichnogenus and ichnospecies for adhesive meniscate burrows (AMB), and paleoenvironmental implications, Paleogene Willwood Formation, Bighorn Basin, Wyoming. Journal of Paleontology, 82(2): 267-278.

Smith, J.J., Hasiotis, S.T., Kraus, M.J. and Woody, D.T., 2009. Transient dwarfism of soil fauna during the Paleocene–Eocene Thermal Maximum. Proceedings of the National Academy of Sciences, 106(42): 17655-17660.

Stein, J.K., 1983. Earthworm Activity: A Source of Potential Disturbance of Archaeological Sediments. American Antiquity, 48(2): 277-289.

Stoops, G., 2003. Guidelines for Analysis and Description of Soil and Regolith Thin Sections. Soil Science Society of America, Inc., Madison, Wisconsin, 184 pp.

Taylor, A., and Goldring, R., 1993. Description and analysis of bioturbation and ichnofabric. Journal of the Geological Society London, 150(1): 141-148.

Thorp, J., 1949. Effects of Certain Animals that Live in Soils. The Scientific Monthly, 68(3): 180-191.

Tobin, R.J., 2004a. Ichnology of a late Pleistocene ichnofabric, Nebraska, USA. Palaeogeography Palaeoclimatology Palaeoecology, 215(1-2): 111-123.

Tobin, R.J., 2004b. Taphonomy of ground squirrel remains in a Late Pleistocene ichnofabric, Nebraska, USA. Palaeogeography Palaeoclimatology Palaeoecology, 214(1-2): 125-134.

Twiss, P.C., Suess, E. and Smith, R.M., 1969. Morphological Classification of Grass Phytoliths. Soil Sci Soc Am Proc, 33: 109-115.

Van Nest, J., 2002. The good earthworm: How natural processes preserve upland Archaic archaeological sites of western Illinois, USA. Geoarchaeology-an International Journal, 17(1): 53-90.

Wilding, L.P. and Drees, L.R., 1973. Scanning electron microscopy of opaque opaline forms isolated from forest soils in Ohio. Soil Science Society of America, Proceedings, 37: 674-650.

Woodburn, T.L., Johnson, W.C., Bozarth, S.R., Mason, J.A., and Halfen, A.F., in review. Vegetation dynamics during the Pleistocene-Holocene transition in the central Great Plains, USA.

Figures

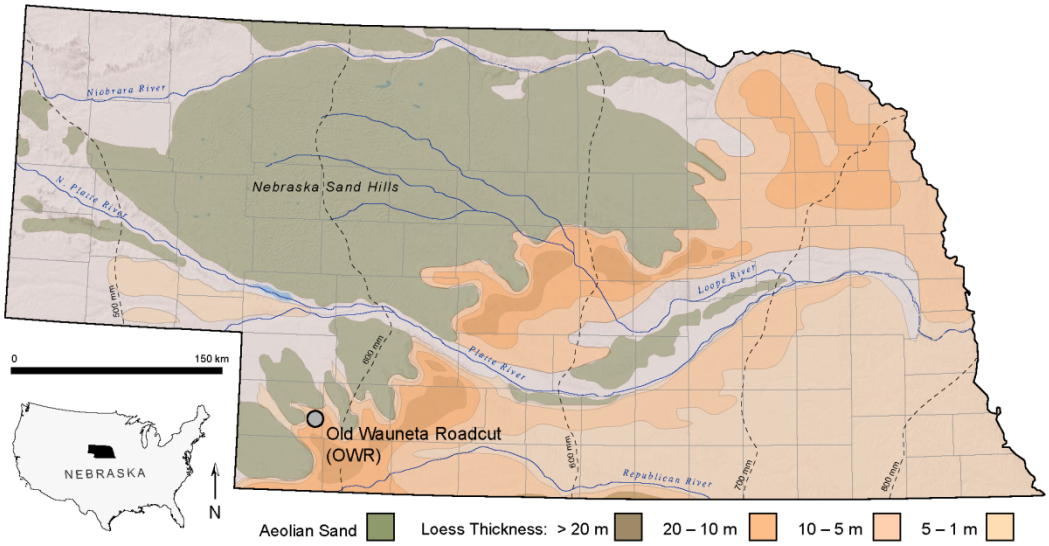

Fig. 1 – Old Wauneta Roadcut location in southwestern Nebraska. Aeolian sand and loess distribution and thickness (produced by Alan F. Halfen, modified from Bettis III et al., 2003).

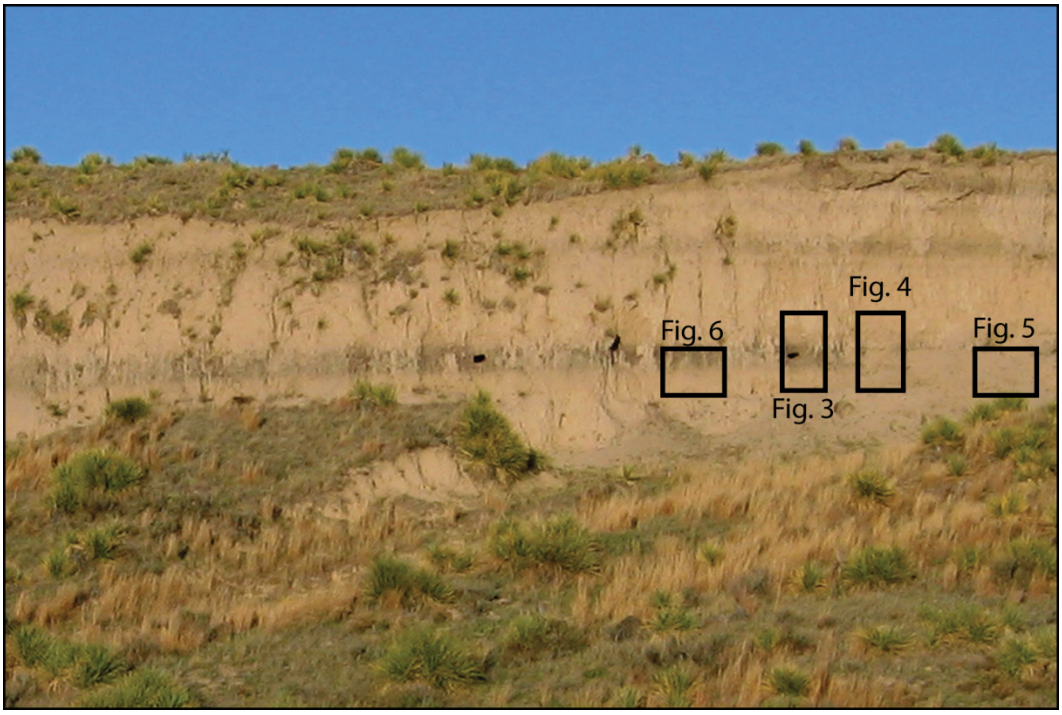

Fig. 2 – Old Wauneta Roadcut image defining profile locations for Figs. 3-6.

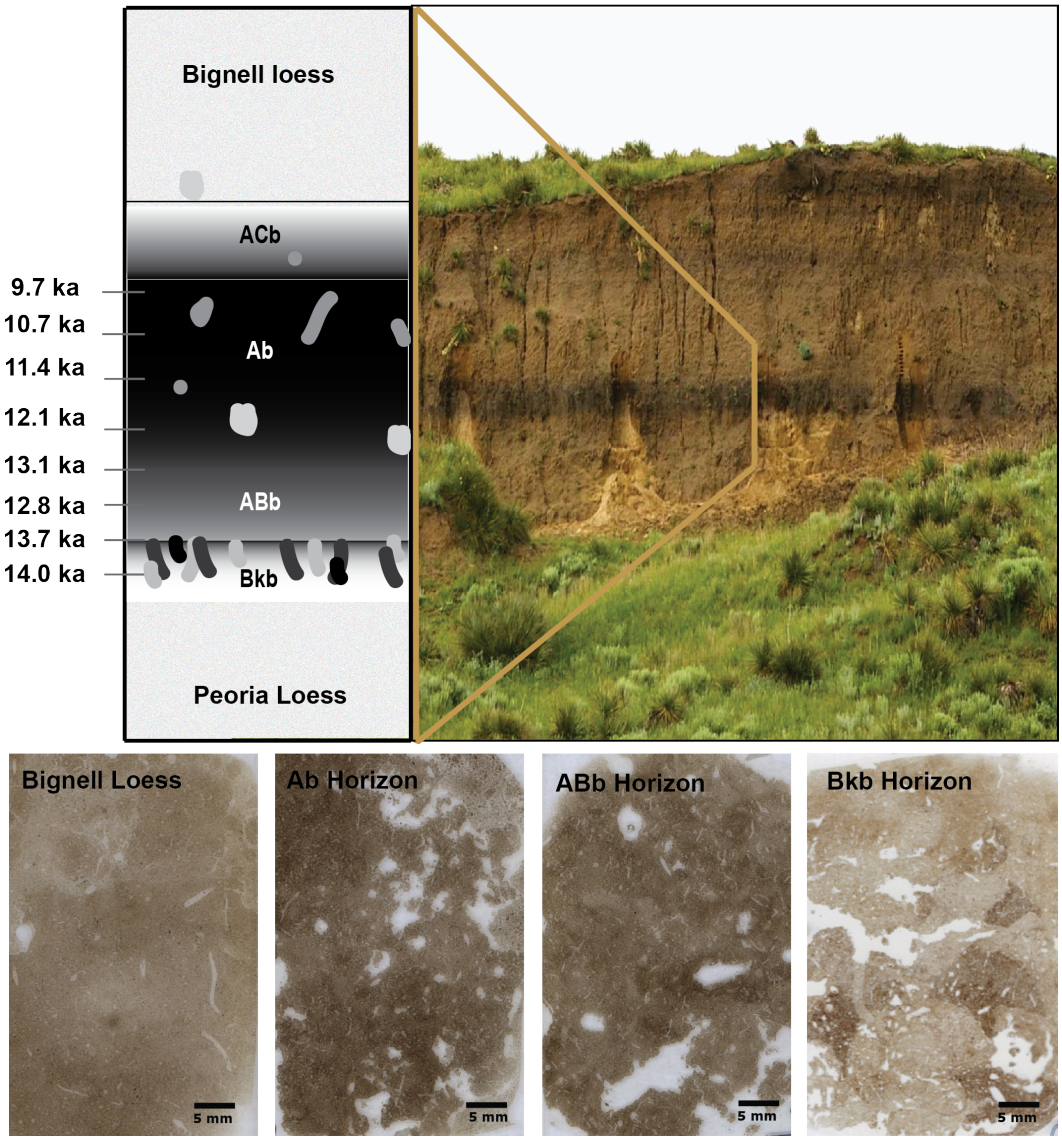

Fig. 3 – Strategraphic profile of the Brady Soil from the Old Wauneta Roadcut exposure characterized by thick, cumulic, organic-rich horizons spaning the Pleistocene-Holocene transition (**c**alibrated radiocarbon ages from Mason et al., 2008). This section slides for the Bignell Loess and Brady Ab, ABb, and Bkb horizons shown below.

E
F
C
B
A
D
Society for Sedimentary Geology
A
Society for
B
C

Fig. 4 – Rodent burrow morphology. A) cross-cutting relationship of two burrows indicated by fill color and texture differences; B) edges of the chamber wall exhibiting effects of invertebrate mixing after infill occurred; C) multiple bioturbation events represented by differences in sediment sources; D) profile of multiple large burrow and chamber systems in the Brady Soil Ab and ABb horizons in reference to a 15cm scale; E and F) examples of thin section slides produced from loess fill within rodent burrows displaying numerous events of subsequent invertebrate mixing.

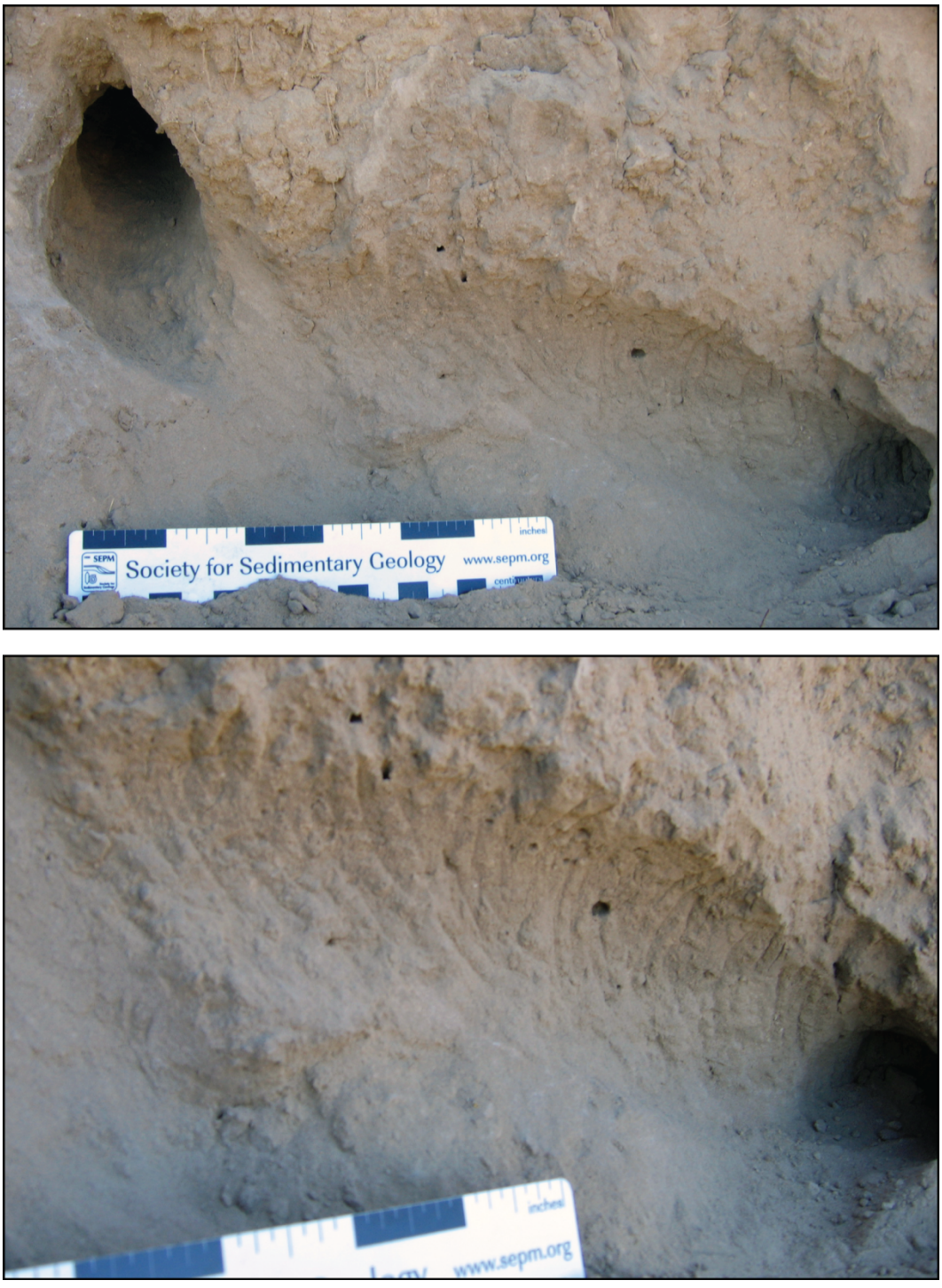

Fig. 5 – Unfilled rodent burrow revealing architecture and rodent scratch marks within the Peoria loess unit. Small, unfilled invertebrate burrows are seen along the wall. Scale represent 15 cm.

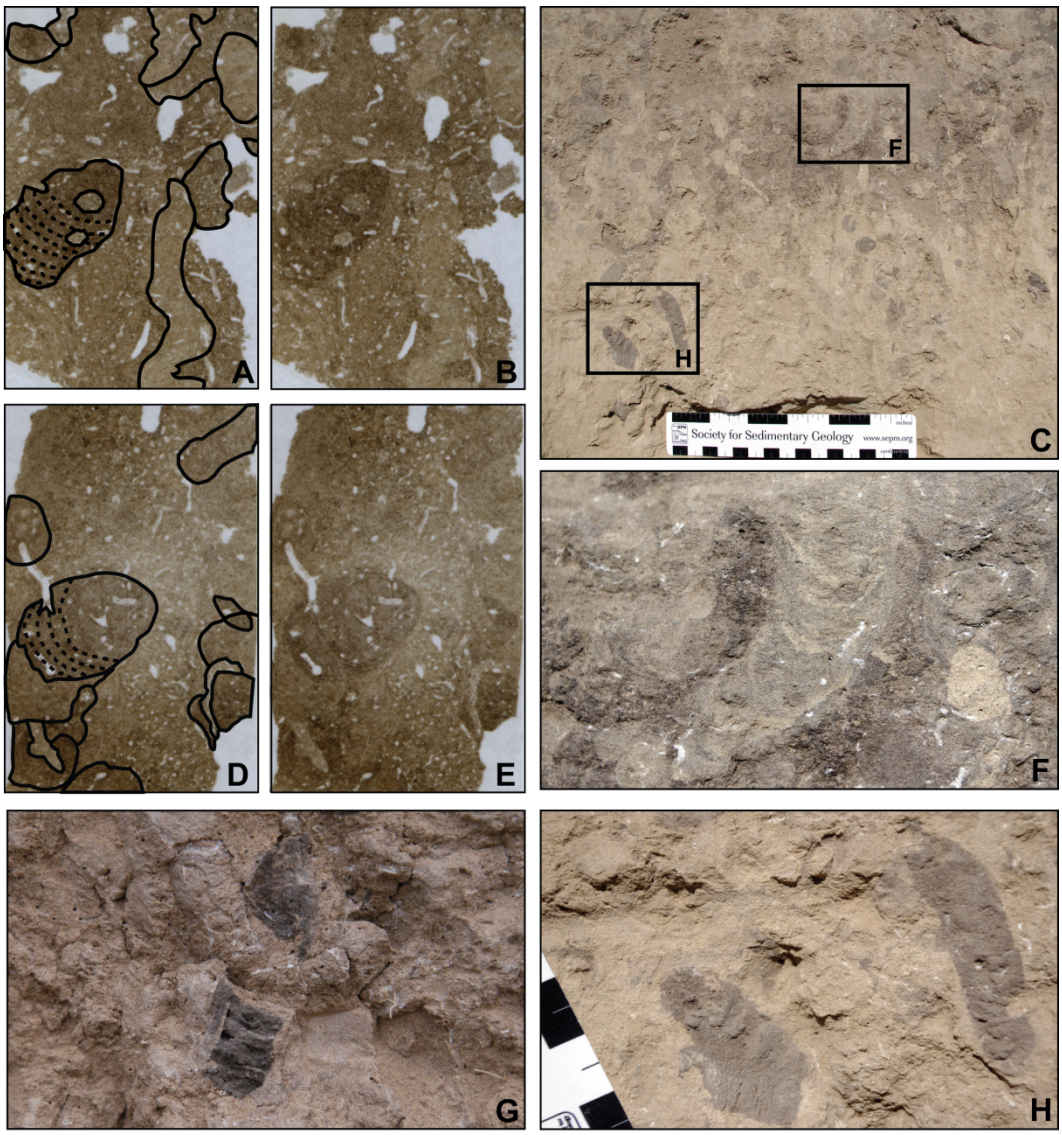

Fig. 6 – *Naktodemasis bowni* ichnotaxon within the ABb and Bkb boundary mixing zone (C) with a 15cm scale. Paired thin sections (A, B and D, E) with and without burrow fill boundaries overlaid, displaying *N. bowni* backfill miniscate and other invertebrate burrows within this boundary location. Close-up views of the distinctive backfill menisci from the soil profile (F, G, and H) indicative of cicada (Cicadidae) nymph or burrower bug (Cydnidea) activity.

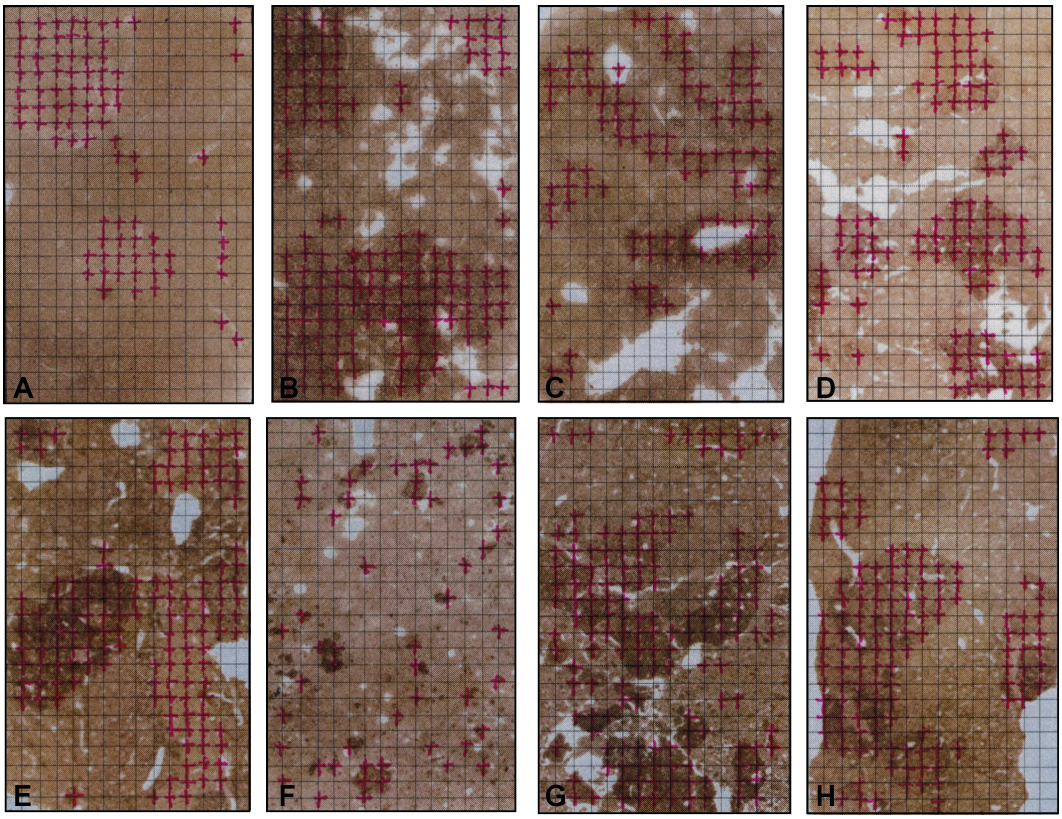

Fig. 7 – Thin section images with grid points marked where traces are met and bioturbation percentages calculated in (A) Bignell Loess 26.4%, (B) Brady Ab horizon 50.7%, (C and G) ABb horizon 33.7% and 48.3% respectively, (D, E, and H) Bkb horizon 36.2%, 44.8%, and 41.6% respectively, and (F) loess fill within rodent burrow 17.3%.

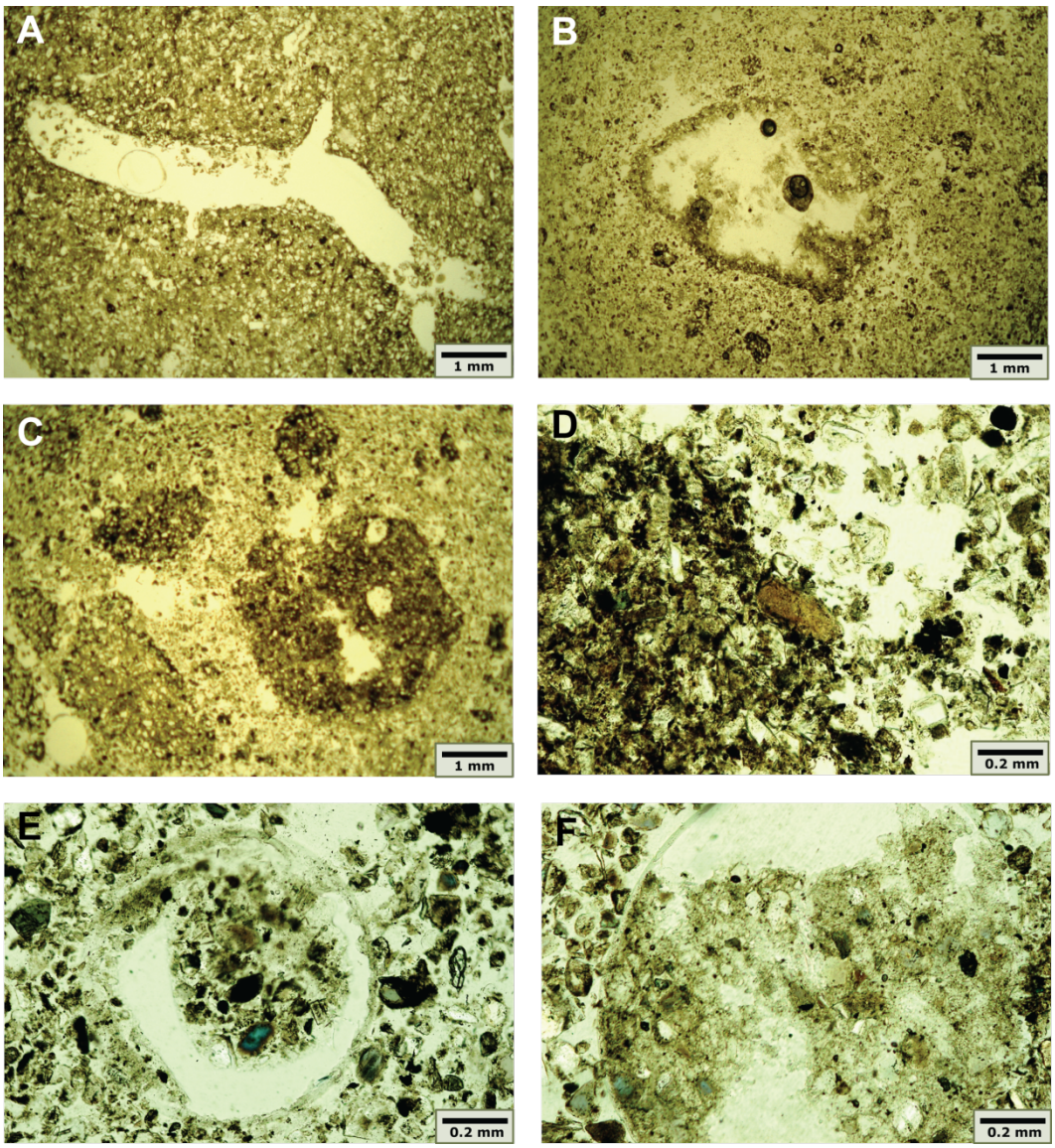

Fig. 8 – Thin section photographs taken at 1x (A, B, C) and 10x (D, E, F) magnifications displaying examples of local (diffusive) mixing events. A) rhizolith showing secondary and tertiary branching patters; B) earthworm reproductive cocoon; C) invertebrate burrows in Bignell loess fill; burrows on right crosscut by roots (round holes); D) edge of organic-rich Naktodemasis in loess sediment; E) decayed root in Peoria Loess with incomplete backfilling or similar material; and F) spongy microstructure of the backfill within a loess root trace.

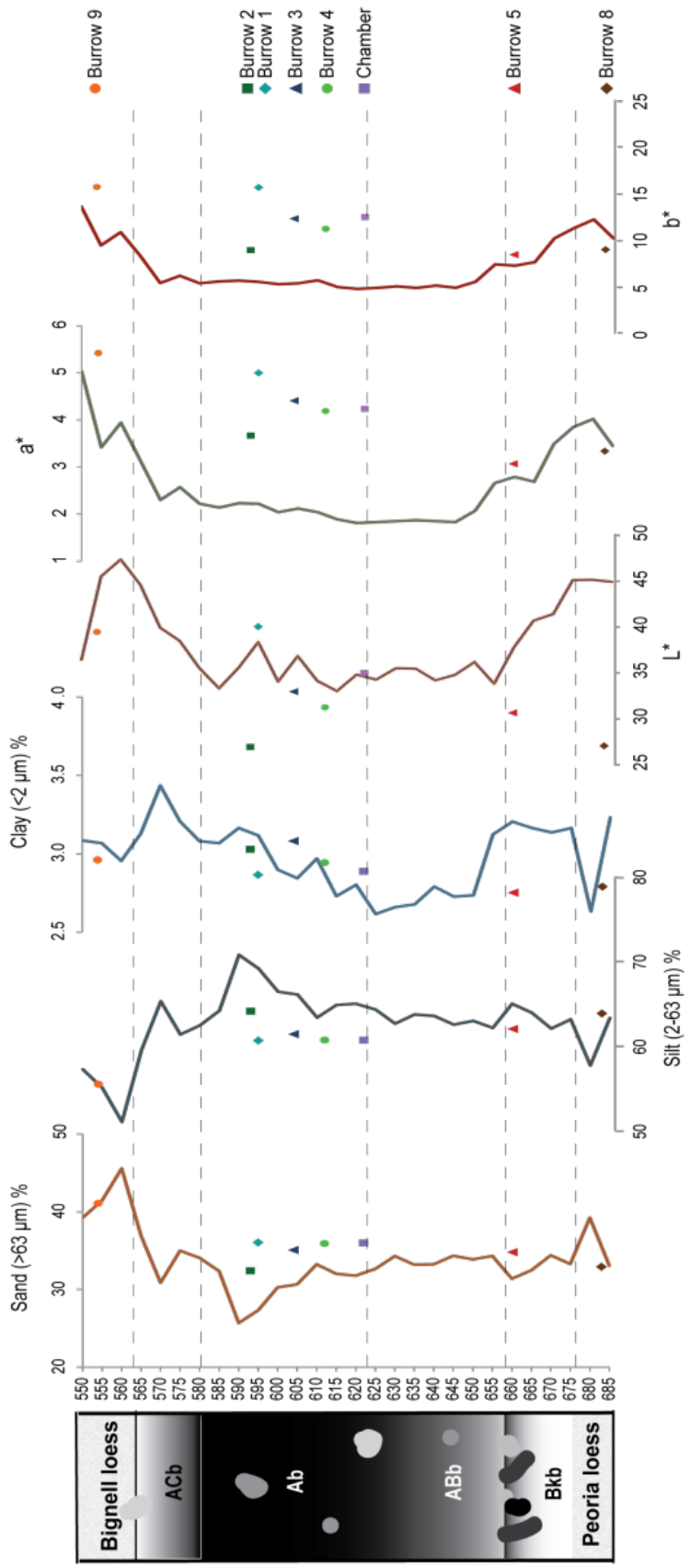
Burrow 9
Burrow 2
Burrow 1
Burrow 3
Burrow 4
Chamber
Burrow 5
Burrow 8
b*
a*
L*
Clay (<2 µm) %
Silt (2-63 µm) %
Sand (>63 µm) %
Bignell loess
ACb
Ab
ABb
Bkb
Peoria loess

Fig. 9 – Particle size distribution and L*a*b color data for the Brady Soil profile and eight burrow samples. Values are shown with respect to the Brady Soil stratigraphy.

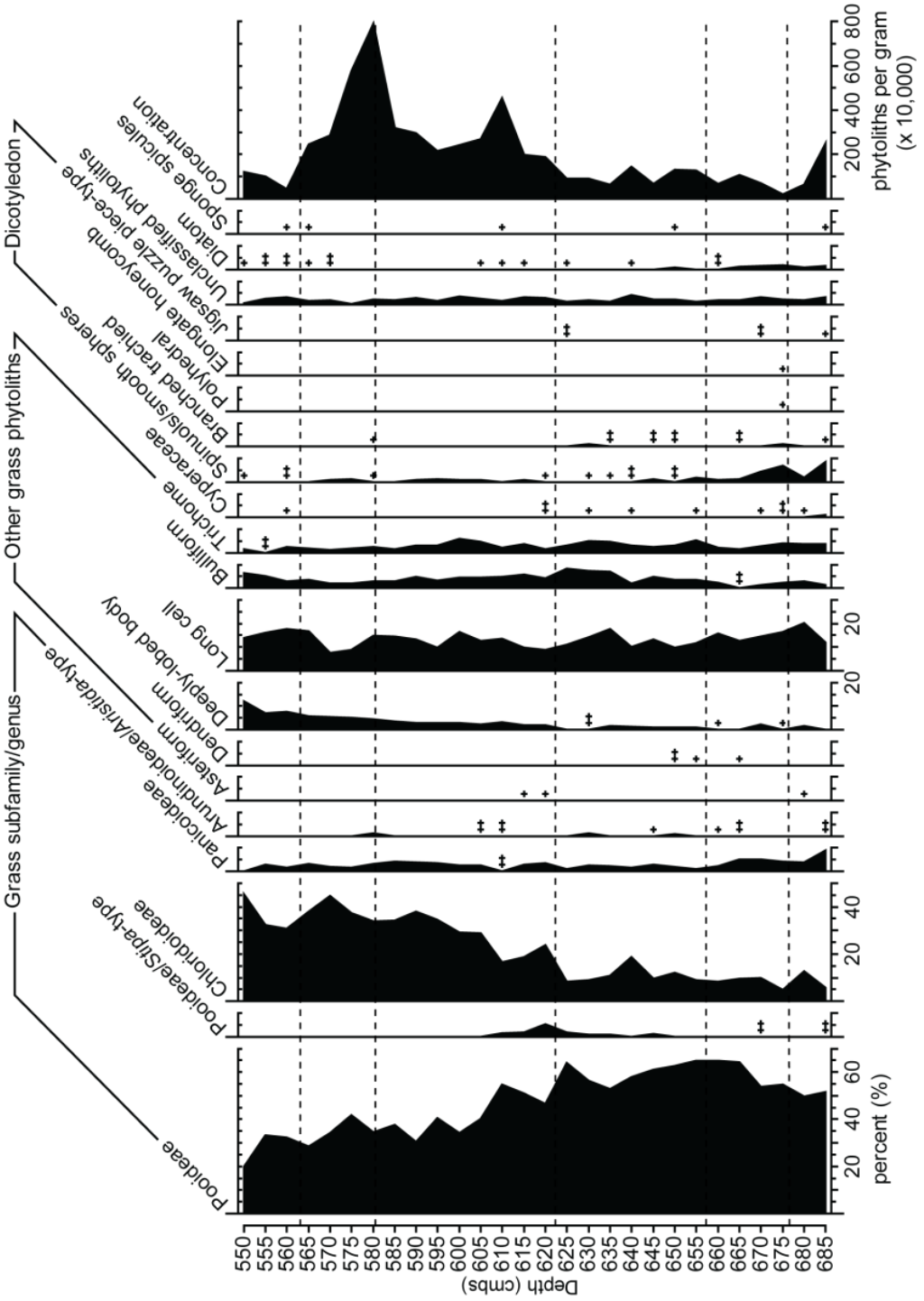
Grass subfamily/genus
Other grass phytoliths
Dicotyledon
Depth (cmbs)
550 555 560 565 570 575 580 585 590 595 600 605 610 615 620 625 630 635 640 645 650 655 660 665 670 675 680 685
Pooideae
percent (%)
20 40 60
Pooideae/Stipa-type
Chloridoideae
20 40
Panicoideae
Arundinoideae/Aristida-type
Asterifrom
Dendriform
Deeply-lobed body
Long cell
20 20
Bulliform
Trichome
Cyperaceae
Spinulos/smooth spheres
Branched tracheid
Polyhedral
Elongate
Jigsaw honeycomb
Unclassified piece-type
Diatom
Sponge spicules
Concentration
200 400 600 800
phytoliths per gram
(x 10,000)

Fig. 10 – Biosilicate frequencies and phytolith concentrations for the twenty-eight samples in the Brady Soil profile. Dashed lines represent Brady Soil pedologic boundaries.

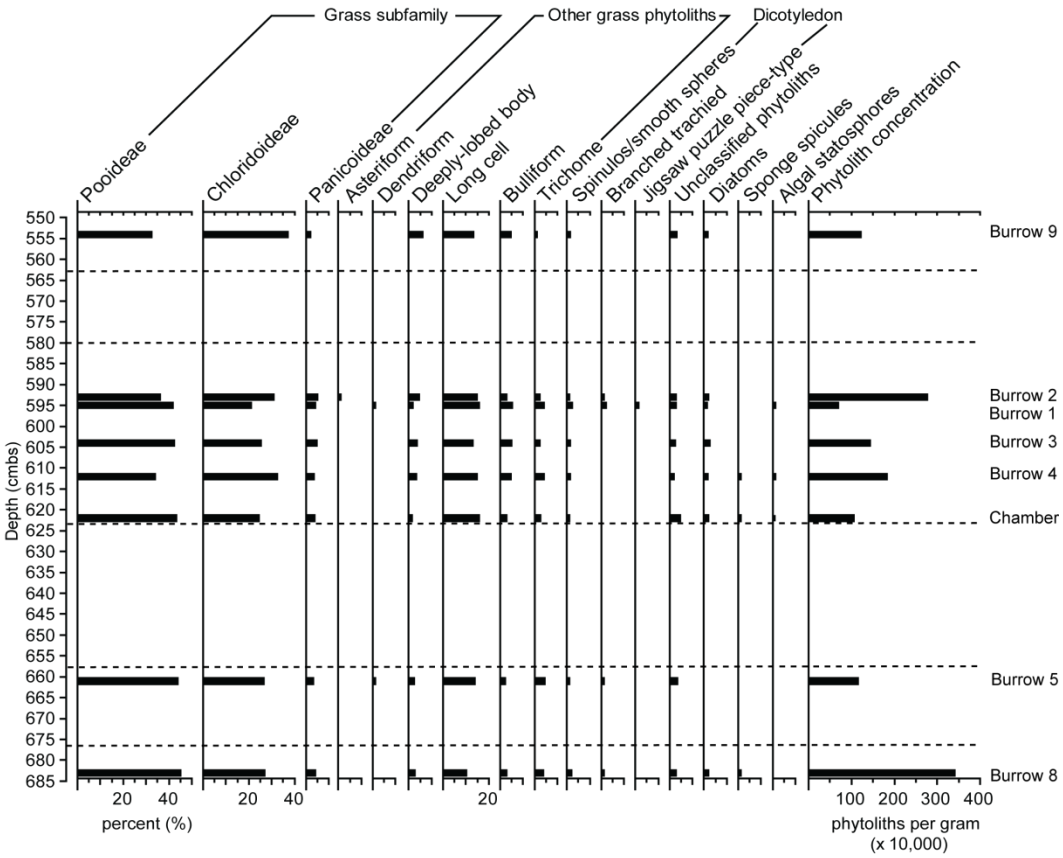

Fig. 11 – Biosilicate frequencies and phytolith concentrations for the eight burrow samples. Dashed lines represent Brady Soil pedologic boundaries.

Chapter 3. Vegetation dynamics during the Pleistocene-Holocene Transition in the central Great Plains, USA

Woodburn, Terri L., Johnson, William C., Bozarth, Steven R., Mason, Joseph A., and Halfen, Alan F. Vegetation dynamics during the Pleistocene-Holocene Transition in the central Great Plains, USA. *Palaeogeography, Palaeoclimatology, Palaeoecology.*

Abstract

The Holocene-Pleistocene Transition in the upland loess mantled regions of the Great Plains is punctuated by an interval of soil formation, the Brady Soil, which separates the late-Pleistocene Peoria Loess and the Holocene Bignell Loess. Previous research of the Brady Soil at the Old Wauneta Roadcut site in Southwestern Nebraska has produced paleoenvironmental reconstructions based on well constrained luminescence and radiocarbon ages, stable carbon isotope ($\delta^{13}C$) analysis of organic matter, magnetic susceptibility, grain size distribution, and L*a*b* color distributions (Mason et al., 2003; Miao et al., 2005; Miao et al., 2007; Mason et al., 2008). While these analyses have shown high effective moisture during formation of the Brady Soil (Mason et al., 2008) and a shift to warm season, C_4 vegetation from the cool season, C_3 dominated vegetation of the Peoria Loess (Miao et al., 2007), data do not provide the necessary detail for full environmental characterizations of this interval. Phytolith analysis provides specific information on paleovegetation communities and shows quantitative shifts of plant taxa that make up these assemblages.

Analysis of short cell phytoliths reveals quantitative plant taxa shifts from Pooideae (C_3) dominant grasses, with relatively large numbers of arboreal dicot spheres

and a few Cyperaceae (sedge) present in a savannah or open woodland setting in the Bølling-Allerød climatic period (~14.6 ka to 12.9 ka), to a mixed, open grassland of Chloridoideae (C_4) and Pooideae (C_3) in the early Holocene. *Stipa*-type Pooideae, a cool-season grass preferring drier soil conditions, marks the onset of the Younger Dryas (~12.9 ka to 11.7 ka), which was previously not revealed in $\delta^{13}C$ analysis. Beyond the quantified changes in vegetation assemblages seen with short cell phytolith analysis, large-cell phytoliths such as long cells, bulliforms, and trichomes, along with other biosilicates, have been shown to be notable climatic indicators in this study. Collective decreases in bulliform, trichome and long cell counts within both C_3- and C_4-dominated temperature phases indicate periods of lower moisture availability and play a major role in climate index calculations. Bulliforms are produced during high evapotranspiration episodes and, therefore, when compared to long cell counts, a water stress index can be computed and used to formulate potential evapotranspiration evaluations. Other biosilicates such as diatoms and sponge spicules typically provide indications of standing water environments. In this study, however, these have been identified primarily within the uppermost solum during the onset of Bignell Loess deposition indicated by lower phytolith concentrations and soil morphology changes. The combination of biosilicate information and concentration values indicates loess influx to the upland from nearby stream valley rather than standing water occurring at the sample site. These data illustrate the need for all grass phytoliths and other biosilicates to be identified, which allows for a more accurate and detailed paleoclimatic reconstruction than would have been possible with bulk sediment-derived $\delta^{13}C$ data, or even with a short cell phytolith data alone.

1. Introduction

The Pleistocene-Holocene Transition (PHT) was a time of rapidly changing climatic conditions associated with the final stages of deglaciation in the Northern Hemisphere (e.g., Alley, 2000; Zielinski and Mershon, 1997). Ice cores have yielded a great deal of high-resolution paleoenvironmental information depicting the PHT in the North Atlantic, leading to a better understanding of these abrupt climate change events (e.g., Alley, 2000; Orombelli et al., 2010; Zielinski and Mershon, 1997). North Atlantic climate in the late Pleistocene has been characterized by a warm Bølling-Allerød (B-A; ~14.7-12.65 cal ka) and a cold, arid Younger Dryas (YD; ~12.65-11.5 cal ka) nearing full glacial conditions, transitioning back to warm conditions in the early Holocene (Zielinski and Mershon, 1997; Björck et al., 1998). YD cooling has been linked to a temporally and spatially expanded polar vortex, which also increased the strength of the westerly wind flow, whereas warming in the early Holocene is likely the result of expanded subtropical high circulation systems due to greater seasonality of temperatures (Zielinski and Mershon, 1997; Alley, 2000). These large and rapid climate fluctuations in the North Atlantic resulted from complex system interconnections, all of which are plausibly related to oceanic heat transfer variability (Alley, 2000). Complex climate interactions, however, can create diverse environmental conditions throughout the Northern Hemisphere and local expressions of the PHT climatic changes in continental interiors are often lacking in detail.

An immense repository of data for the Quaternary and window into climatic patterns of the interior North American continent is provided by loess-paleosol stratigraphy on the central Great Plains. Late Pleistocene and Holocene loess of this region is thickest in south-central Nebraska, just south of the Nebraska Sand Hills (Fig. 1), decreasing in thickness into Kansas and northeastern Colorado (Thorp and Smith,

1952; Kollmorgen, 1963; Mason, 1998, 2001; Bettis III et al., 2003). Sediment producing the loess is from the dry dunefields, but additions were also derived locally from glacially affected fluvial systems (Mason, 2001; Mason et al., 2008; Muhs et al., 2008). This silt sediment originated primarily from weathering of the White River Group, Arikaree Group, and the Pliocene bed siltstones found northwest of the local area in the Badlands region (Muhs et al., 2008). The record of late-Quaternary loess deposition consisted of five major periods of instability and rapid deposition: pre-Illinoian pre-Loveland loess (undifferentiated), Illinoian Loveland Loess, middle-Wisconsinan Gilman Canyon Formation, late-Wisconsinan Peoria Loess, and Holocene Bignell Loess, interspersed with periods of soil formation (Fig. 2; Baars and Maples, 1998; Johnson and Willey, 2000). The Brady Soil (Schultz and Stout, 1948), formed during an interval of well-defined upland pedogenesis, encases the PHT and separates the Peoria and Bignell loess units (Fig. 2). Age estimates presented in this paper are calibrated radiocarbon ages in thousands of calendar years before present.

Brady Soil formation is time transgressive over the Great Plains region. Mason et al. (2008) have constrained the beginning of Brady pedogenesis to ~14.7 to 13.5 cal ka and termination ~9 cal ka. Pedogenesis, therefore, occurred through the end of the late Pleistocene (through both the B-A and YD) and continued over 2,000 years into the early Holocene. Reconstructions of the PHT using information derived from the Brady Soil show a general trend of warming and drying from the late Pleistocene into the early Holocene, based primarily on stable carbon isotope ($\delta^{13}C$) shifts from C_3- to C_4-dominant vegetation (Johnson and Willey, 2000; Jacobs and Mason, 2004; Miao et al., 2007; Mason et al., 2008). Cordova et al. (2011) linked the dominance of C_3 plants in the late Pleistocene to decreased summer precipitation due to diminished subtropical air flow and

associated the warming trend in the early Holocene to increased seasonality and higher summer temperatures as a result of orbital forcing.

Few locations, however, are able to characterize the YD interval for the Great Plains because the interval is not always expressed as a specific litho- or biostratigraphic unit, though available data have concluded a warming and drying trend and possibly a short-lived increase in aeolian activity during the YD (Mason et al., 2008; Holliday et al., 2011). The YD signal on the Great Plains differs greatly from the cold, near full-glacial conditions of the North Atlantic region, but records from both regions have indicated a similar drying trend. Increased dust influx occurs in the ice record of the North Atlantic (Zielinski and Mershon, 1997) and has also been noted at a few locations on the Great Plains, though it has not been found to be a spatially extensive response to aridity during the YD (Mason et al., 2008).

Use of soil $\delta^{13}C$ is prevalent in many regions beyond the North American Great Plains due to its relative ease of analysis. For example, researchers in Africa (e.g., Cerling, 1984; Wynn, 2000; Roberts et al., 2013) and China (e.g., Frakes and Jianzhong, 1994; Liu et al., 2005; Wang et al., 2008; Zhou, 2009) have used this climatic proxy. In the central Great Plains, use of stable carbon isotope values has become pedestrian, e.g., Feggestad et al. (2004), Miao et al. (2007), and Mason et al. (2008) in Nebraska; and Arbogast and Johnson (1998), Johnson and Willey (2000) and Cordova et al. (2011) in Kansas. In a synthesis of carbon isotope data from surface and buried soils previously reported for the North American Great Plains, Nordt et al. (2007) reconstructed July mean temperatures.

A limitation of the $\delta^{13}C$ climatic proxy is the generalized designation of vegetation as C_3, C_4, or mixed flora types without discriminating between woody

vegetation and cool-season grasses. Global studies have been attempting to move beyond $\delta^{13}C$ vegetation reconstructions by using the more time intensive pollen or phytolith analyses to produce distinct vegetation assemblages with family or genus-level information (e.g., Alexandre et al., 1997; Bremond et al., 2005; Barboni et al., 2007; Lu et al., 2006; Garnier, 2013; Magill et al., 2013)

Extraction of proxy records of vegetation change beyond that of $\delta^{13}C$ has been challenging in the central Great Plains, mainly due to the lack of natural lake catchments for quality fossil pollen preservation. However, biogenic soil microfossils, such as phytoliths and other biosilicates, present an optimal resource for paleoenvironmental reconstructions in the Great Plains where grasses predominate and fossil pollen grains are inconsistently preserved. The few paleoenvironmental reconstructions for this region have been derived using phytolith analysis (e.g., Twiss, 1983; Fredlund et al., 1985; Kurmann, 1985; Bozarth, 1992; Fredlund and Tieszen, 1994; Fredlund and Tieszen, 1997; Cordova et al., 2011), and only one study has attempted to reconstructed the PHT through the Brady Soil (Bozarth, 1998).

Opal phytoliths are microscopic silica bodies formed by the uptake of water and dissolved materials from the soil and subsequent precipitation of silica within or between plant cells (Piperno, 1988; Mulholland and Rapp Jr., 1992a; Piperno, 2006). Short cell phytoliths in grasses can be identified to subfamily and, occasionally even genus level (Piperno, 2006). Accordingly, opal phytolith analysis is used to quantify paleovegetation assemblages of grass subfamilies (Pooideae, Chlorideae, and Panicoideae) and phytolith types for trees and shrubs. Not only do phytolith frequencies permit the identification of specific changes in vegetation assemblages through time, but they also enhance the knowledge of paleoclimatic features. Such large-cell phytoliths as long cells, bulliforms, and trichomes have often been overlooked in previous phytolith studies in that they are

primarily non-diagnostic phytolith forms, but they have been found useful in determining drought episodes and variations in evapotranspiration rates (Sangster and Parry, 1969; Bremond et al., 2005; Delhon, 2007).

The objective of this paper is to refine the environmental reconstruction of the PHT for the central Great Plains through a relatively high-resolution paleovegetation record for the Brady Soil using biosilicate analyses. Biosilicate classification and tallies allow for a more quantitative reconstruction of vegetation assemblages than that provided by $\delta^{13}C$ data. The goals of using phytolith analysis are to (1) distinguish C_3 plant types of woody plants and cool-season grasses to determine if woody plants grew at this location; (2) ascertain whether or not a Younger Dryas climate response can be acquired with this proxy; and (3) determine relative temperature and moisture conditions through the PHT, as well as, defining the extent of vegetation change.

2. Study site

Selection of the Old Wauneta Roadcut site (40.500561° N, 101.417872° W; ~1017 m amsl) was a function of its location along the edge of a thick loess deposit that contained a clearly-expressed Brady Soil (Fig. 1, 3), and to availability of data from previous investigations, including detailed age constraints of the Brady Soil (Jacobs and Mason, 2004; Miao et al., 2005; Mason et al., 2008). The site is the road cut of an abandoned county road located ~10 km northwest of the town of Wauneta in Chase County, Nebraska and ~75 km south of the North and South Platte River valleys (Fig. 1). Modern climate characteristics, as recorded at Wauneta, NE, include a January mean temperature of -1.3°C, a July mean temperature of 25.7°C, and mean annual precipitation of 493 mm with the majority of the precipitation occurring in summer months (HPRCC, 2013). Vegetative cover consists of a mixed-grass prairie with a variety of prairie-

community forbs. The abandoned roadcut sits on a topographical high at the northern edge of a loess-mantled upland (regionally referred to as "tables"), with the broad valley of Spring Creek to the north. The site consists of a west-facing, vertical cut that exposes late-Quaternary stratigraphy including the late-Wisconsinan Peoria Loess and Holocene Bignell Loess, which are separated by the Brady Soil, formed within the uppermost Peoria Loess during the PHT (Figs. 2, 3; Baars and Maples, 1998).

3. Methods

A profile of the roadcut exposure was excavated back to a fresh surface, measured, described and otherwise documented, and then sampled for stable-carbon isotope and phytolith analysis. Discrete 5-cm samples were collected starting in the uppermost portion of the Peoria Loess, through the Brady Soil, and ending in the lowermost portion of the Bignell Loess. Though stable carbon isotope ($\delta^{13}C$) data for the Brady Soil at the Old Wauneta Roadcut were reported by Miao et al. (2007), $\delta^{13}C$ were derived from the samples in this study for direct comparison to phytolith frequencies. Preparation for $\delta^{13}C$ and percent organic carbon measurements included removal of roots and other organic debris by hand picking, and removal of carbonates by treating samples with 1M HCl and rinsing until a pH of 5 was obtained. Isotopic analyses were completed by the University of Kansas W.M. Keck Paleoenvironmental and Environmental Stable Isotope Laboratory (KPESIL) using a Costech Elemental Analyzer to evaluate organic carbon content through combustion and a ThermoFinnigan MAT 253 isotope ratio mass spectrometer to determine raw $\delta^{13}C$ values. A calibration curve was produced using soil, peach-leaf, and yeast standards to provide corrected $\delta^{13}C_{VPDB}$ values.

Phytoliths and other biosilicates were extracted from 5 g of sediment after dissolution of carbonates using 10% HCL, clay removal, oxidation of organic matter

using 30% H_2O_2 (heated in a hot water bath until reaction subsided), and separation of biosilicates from most other mineral matter using a $ZnBr_2$ (d = 2.3) heavy-liquid floatation (Bozarth, 2008; Appendix A). Samples were mounted on microscope slides in immersion oil to allow for three-dimensional observation. Transects were scanned until ≥200 shortcell phytoliths were counted and identified. Diagnostic grass shortcells consist of shapes described as bilobate, cross, saddle, and trapezoid, each with many variations, were identified according to Twiss et al. (1969), Brown (1984), and Mulholland and Rapp Jr. (1992b). Distinguishable dicotyledon (tree and shrub) phytolith morphologies include spheres, polyhedrons, jigsaw-puzzle type, honeycomb assemblages, branched tracheids, segmented hairs, scalloped phytoliths, and platelets, and were classified based on descriptions by Bozarth (1992) and Wilding and Drees (1973). Additional biosilicates, such as large cell phytoliths, sponge spicules, and diatoms, were tallied during microscopic analysis as supplementary proxy data. Frequency records were rendered in graphical format using the Tilia program (Grimm, 2011) with assemblages displayed as percentages of the sum of all biosilicates.

Paleoenvironmental conditions have been expressed as three indices: (1) a C_3:C_4 grassland ratio derived from frequencies of short-cell grass phytoliths as described by Twiss (1987); (2) a Bulliform Index showing water stress due to evapotranspiration as described by Delhon (2007), and (3) a proposed Soil Moisture Index derived from large cell (bulliforms, trichomes, and long cells) grass phytolith frequencies plus the short-cell phytoliths. All indices are calculated from raw phytolith counts and based on a scale of 0 to 1. The C_3:C_4 grassland ratio compares Pooideae to a sum of all short-cell phytoliths to express temperature characteristics. Values approaching 1 correlate to Pooideae-dominated (C_3) cool-season grasslands, while values closer to zero are associated with warm-season Chloridoideae-dominated (C_4) grasslands. The Bulliform Index (BI) is the

ratio of bulliform phytoliths to long-cell (elongated) phytoliths and is based on the fact that silicification of larger cells requires greater soil moisture availability to facilitate an increase in dissolved silica uptake (Delhon, 2007). An increase in temperature, in combination with greater soil moisture availability, will create an environment with increased evapotranspiration of water through the bulliform cells of a plant, leading to higher counts of bulliform phytoliths (Sangster and Parry, 1969; Delhon, 2007). Greater evapotranspiration, or water stress, therefore, will be designated by higher BI values, i.e., those approaching 1. The premise that greater soil moisture allows for large-cell phytolith development was also exploited to create a Soil Moisture Index (SMI), which uses both short- and large-cell phytoliths to account for moisture availability from the atmosphere as well as from soil storage. The SMI is a modification of the aridity index originally introduced by Twiss (1987), who interpreted moisture levels based on Chloridoideae frequiencies divided by the sum of short-cell phytoliths. More recent work on the distribution, phylogeny, and climate space of C_4 grasses indicates, however, that the Twiss (1987) ratio is more reflective of temperature conditions (Edwards and Still, 2008), similar to the C_3:C_4 grassland ratio. The SMI calculation uses Panicoideae (C_4 grass) frequencies to indicate the humid climate and/or high available soil moisture content required for growth (Twiss, 1987; Bremond et al., 2005), instead of representing warm temperatures. The SMI also takes into consideration genus-level grasses that indicate moisture availability. In this study area the *Stipa*-type Pooideae was observed, which is indicative of a cool season (C_3) grass that grows in arid conditions (Pohl, 1954). The formulation used herein is the ratio of: Chloridoideae + *Stipa*-type / Chloridoideae + *Stipa*-type + Panicoideae + Pooideae + longcells + trichomes + bulliforms. SMI values range from 0 to 1 with higher values indicating low moisture availability.

4. Results

4.1. Stratigraphy

The Brady Soil at the study site is a well-developed, cumulic soil (cf. Fine, smectitic, mesic Typic Argiustolls) with a solum ≥ 1 m thick, which began to develop as deposition of Peoria Loess diminished. At the sampled profile the surface of the Ab horizon begins ~580 cm below the modern surface, though above this is an ACb horizon, which presumably reflects pedogenesis being extinguished by the initiation of Bignell loess deposition. The dark colored (~10YR 3/1 moist) Ab horizon transitions into an ABb horizon that remains similarly dark in color (~10YR 4/1 moist), but displays slight carbonate content. Dark A-horizon colors correlate to increased soil carbon percentages and perhaps somewhat to increase concentrations of particulate charcoal (Fig. 4). A continued pickup in illuvial clay and carbonate content occurs at the base of the solum in the Bkb horizon, which displays a slight shift to yellower hue (~0.3Y 4/2 moist) than overlying A horizons and decreased soil carbon concentrations similar to those of the Peoria Loess (Fig. 4).

4.2. Phytolith and isotope analyses

Twenty-eight samples were examined to produce a relatively high-resolution vegetation reconstruction through the PHT (Fig. 5; Appendix B). A stratigraphically constrained cluster analysis of phytolith frequencies (CONISS) (Grimm, 1987), performed in Tilia, displayed three major zones of vegetation assemblages. These zones correspond with the timing of North Atlantic climate episode chronostratigraphy, the Pleistocene Bølling-Allerød (B-A), Pleistocene Younger Dryas (YD), and the early Holocene based on the distribution of calibrated radiocarbon ages obtained from Mason et al. (2008) (Figs. 4, 5). Both $\delta^{13}C$ and phytolith counts indicate a mixed C_3/C_4 signal

through the PHT, with C_3 dominance in the late Pleistocene and C_4 grasses increasing in the early Holocene, though phytolith analysis established that late-Pleistocene B-A vegetation has a greater C_3 dominance than indicated by $\delta^{13}C$.

5. Discussion

5.1. Considerations for proxy interpretation

With any proxy analysis there are issues to be considered before paleoenvironmental reconstructions can be confidently established. For the Brady Soil at the Old Wauneta Roadcut, the mixing of sediment by bioturbation requires examination. Moderate to large burrow systems are visible within the soil profile and bounding loess units, and are usually visible and can be avoided through careful sampling. A bulk, 5-cm sample size was chosen for this site due to the visible evidence of a ~5 cm mixing depth of high-density, small burrows that are difficult to avoid during sampling. Through observation and experimentation, this sampling approach provides a relatively high-resolution account of environmental properties without displaying mixing signals. Mixing within soil horizons is not always easily detectable, however, and the approach to site assessment must be adjusted accordingly in heavily bioturbated soils. Pairing phytolith analysis with more generalized climate proxies, such as $\delta^{13}C$, and with the chronostratigraphy of Mason et al. (2008), provides substantiation of stratigraphic integrity. Age values are in sequence with the exception of the anomalous age of 12.8 ka within the B-A. However, matching the stratigraphy to other studies of this site (Mason et al., 2008; Miao et al., 2007), the placement of B-A, YD, and early Holocene age classifications are appropriate. A thorough examination of bioturbation at this site is presented in a separate study by Woodburn, Hasiotis, and Johnson (in preparation).

5.2. Vegetation dynamics

Stable carbon isotope data correlate well to the general trends of C_3 and C_4 phytolith frequencies. Moreover, the use of phytolith analysis provided the capacity to distinguish C_3 plant types of cool-season grasses and woody plants, as well as to provide quantitative shifts in vegetation assemblages. Paleoenvironment indices constructed using phytolith information added the ability to detect subtle climatic adjustments, thereby further articulating the nature of the environmental change.

Phytolith analysis showed that the C_3 signal in the late Pleistocene B-A is due largely to cool-season Pooideae grasses that produce trapezoidal short-cells, as well as to the presence of trees and shrubs as indicated by spheres, branched trachieds, and other dicotyledon phytolith types (Fig. 5). Phytoliths from woody plants are indicated typically as rare types due to underrepresentation in the phytolith record (Piperno, 2006). Dicotyledons produce low quantities of silica bodies and some types such as the thin, fragile polyhedral-type phytoliths are poorly preserved (Piperno, 2006). Consequently, an increased frequency of woody plant phytoliths denotes a change from open grassland to a more wooded vegetation structure. Moreover, within the Bkb horizon (at the depth of 675 cmbs), elongated honeycomb and polyhedral-type phytoliths were identified thereby representing the presence of deciduous trees (Fig. 5), an indication of greater moisture availability during the B-A.

Pooideae (C_3) grass dominance continues to be prevalent through the YD, which signifies cool temperatures, but an increase in Chloridoideae (C_4) grasses occurs for a short interval, as recorded from the sample taken at 620 cmbs (Fig. 5). An associated peak in *Stipa*-type (a cool-season Pooideae grass that grows in arid environments) bilobate phytoliths suggests, however a decrease in moisture conditions rather than a

significant temperature increase at this time. The peak in *Stipa* is also coeval with slight decreases in long cell phytoliths within the YD, thereby corroborating lower moisture availability. In the early Holocene, a further increase in warm-season (C_4) Chloridoideae grasses, shown by greater counts of squat saddle-shaped phytoliths and reduced concentrations of dicotyledon phytoliths, characterize a warming and drying trend.

Low counts of Cyperaceae (sedge) cone phytoliths and diatom biosilicates (found only as small, broken pieces) occur at similar depths to one another within the profile (Fig. 5). Their highest frequencies appear in two intervals of differing environmental conditions: the cool, moist Pleistocene B-A (when Brady soil formation was commencing) and the warm, dry early Holocene (when soil formation was ending). These times of occurrence correspond to the highest rates of sediment input during the end of the Peoria loess deposition within the Bkb and ABb horizons of the Brady Soil, and during the onset of Bignell loess deposition (Fig. 5). In this setting, Cyperaceae and diatoms may, in fact, be markers for increased loess sediment influx, in that they were transported with the aeolian sediment originating from the adjacent Spring Creek valley and/or the Platte River valley to the north.

High moisture availability during the late Pleistocene, indicated by the low values of the soil moisture index (Fig. 4), denotes mesic conditions at this time, as do the Pooideae-dominated grasses and woody vegetation. Evapotranspiration rates signified by the BI (Fig. 4) are lowest in the Bkb soil horizon during the late Pleistocene when woody vegetation was at its peak. The SMI shifts to exhibit moderate and drier conditions as soil production continues into the Holocene, with a rapid drying trend in the middle of the YD. Evapotranspiration hits two high points during the beginning and near the end of the YD, yet the vegetation assemblage was still dominated by C_3 types due to sufficient levels of moisture still available during these periods. Since C_3 grasses retain their

dominance during the early and late YD, an increase in temperature must have occurred to force the increase in evapotranspiration. Conversely, during the B-A and YD there are decreases in evapotranspiration that correspond to relatively short periods of increased aridity. These lowered rates in evapotranspiration during times of drought occur due to short-term changes in vegetation, such as the peak in Chloridoideae in the B-A and YD (at 640 and 620 cmbs), and in drought-tolerant *Stipa*-type Pooideae in the YD (at 620 cmbs) (Figs. 4, 5). These vegetation types use moisture more effectively, thus BI values are lowered in times when cooler temperatures are not the controlling factor. Similarly, the overall decrease in evapotranspiration seen with warming temperatures in the early Holocene is partially controlled by the increase of C_4 Chloridoideae vegetation. Though, the nearly equivalent concentrations of cool-season Pooideae and warm-season Chloridoideae during the Holocene imply an increased seasonality with increased summer temperatures. The formation of a rainy season is also suggested. It is probable that soil moisture retention during and after the rainy season is greater due to an increase in soil-water-storage capacity in the Ab horizon, as supported by the similar levels of Panicoideae during both the late Pleistocene and Holocene. These conditions would allow for the high percentage of Pooideae grasses to continue thriving in a warmer climate. During the termination of Brady Soil pedogenesis, evapotranspiration rates increase once again with the increases in temperature and corresponding aridity, and with the acceleration of Bignell loess deposition (Fig. 4).

6. Conclusions

Data provided herein represents the first known paleovegetation reconstruction of the Brady Soil using phytolith analysis. Use of phytolith frequencies in concert with multiple paleoenvironmental indices provides detailed vegetation characteristics in loess-

paleosol settings in the absence of fossil pollen records. At the Old Wauneta Roadcut site, the general trend of a cool, mesic Pleistocene transitioning to a warm, dryer Holocene was previously documented with stable carbon isotope data (Miao et al., 2007). Phytolith analysis confirms this trend, but revealed a significant level of additional information. Phytolith data indicate that during the onset of Brady Soil formation in the late Pleistocene Bølling-Allerød the region was savannah to open woodland, subsequently transitioning to an open grassland environment by the early Holocene. Another significant contribution of phytolith analysis to the reconstruction of the environment during Brady Soil time was the documentation of the short-term environmental change during the Younger Dryas, characterized by the distinctive *Stipa*-type Pooideae signal, a decrease in long-cell phytoliths, and dramatic changes in water stress. Hence, phytolith analysis displayed the warming and drying sequences not evident in the $\delta^{13}C$ data.

Supplementary moisture information, obtained through large-cell phytoliths counts and subsequent SMI and BI, revealed shifts in seasonality and occurrence of short or limited intensity drought episodes within larger climate events. As exhibited in these indices, the early Holocene mixed-grass prairie environment indicated a change to greater seasonality, with warmer summers and a rainy season, whereas the onset of Bignell loess deposition occurs coeval with both aridity and temperature increases.

This study provides another level of support to the changing environmental conditions through the PHT, and findings correlate well with others in the central Great Plains (e.g., Cordova et al., 2011; Mason et al., 2008; Miao et al., 2007). The change to warmer and drier conditions occurs gradually in the early Holocene based on similar frequencies of Pooideae and Chloridoideae followed by continued increase of Chloridoideae at the beginning of Bignell loess sedimentation. Enhanced seasonality and

the increase of C_4 grasses in the early Holocene are similar to the trend reported by Cordova et al. (2011), however this shift occurred earlier in southwestern Nebraska than the 10.2 cal ka reported at Kansas sites. The onset of this climate transition occurs more than 2,000 years prior to the end of Brady Soil formation, yet stable surface conditions and pedogenesis continues during this time of increased aridity. Mason et al. (2008) attributed the mature nature of the Brady soil to an extended period of high effective moisture across the PHT. Climate indices produced from phytolith data have shown that the B-A had high moisture availability paired with relatively low evapotranspiration rates. Lower precipitation characterizes the period of early Holocene pedogenesis, yet available soil moisture slightly offsets decreased precipitation. Low evapotranspiration rates persisted in the early Holocene due to an increase in C_4 grass concentrations. Both of these situations describe environments with the effective moisture sufficient for pedogenesis. Increased water stress on plants and a spike in aridity noted during the YD are environmental conditions that support the possibility for a brief rejuvenation of loess sedimentation postulated by Mason et al. (2008). Based on phytolith concentrations, surface conditions are most stable in the early Holocene immediately following the YD, continuing to the surface of the Ab horizon at 580 cm when loess influx rates increase once more (Fig. 5). During Bignell loess deposition, the dramatic increase in aridity coupled with increased evapotranspiration rates leads to an environment of low effective moisture and surface instability ensues.

Acknowledgements

Financial support for this work was provided by the University of Kansas General Research Fund and Kollmorgen Fellowship Award from the University of Kansas Department of Geography. We are grateful to the landowners for permitting us to make repeated visits to the site.

References

Alexandre, A., Meunier, J.D., Lezine, A.M., Vincens, A., and Schwartz, D., 1997. Phytoliths: indicators of grassland dynamics during the late Holocene in intertropical Africa.

Alley, R.B., 2000. The Younger Dryas cold interval as viewed from central Greenland. Quaternary Science Review, 19: 213-226.

Arbogast, A.F. and *Johnson, W.C.*, 1998, Late-Quaternary Landscape Response to Environmental Change in South-Central Kansas: Association of American Geographers *Annals* 88: 126-145

Baars, D.L. and Maples, C.G. (Editors), 1998. Lexicon of Geologic Names of Kansas (through 1995), Bulletin 231. Kansas Geological Survey, Lawrence, KS.

Barboni, D., Bremond, L., and Bonnefille, R., 2007. Comparative study of modern phytolith assemblages from inter-tropical Africa. Palaeogeography, Palaeoclimatology, Palaeoecology, 246(2-4): 454-470.

Bettis III, E.A., Muhs, D.R., Roberts, H.M. and Wintle, A.G., 2003. Last Glacial loess in the conterminous USA. Quaternary Science Reviews, 22(18-19): 1907-1946.

Björck, S. et al., 1998. An event stratigraphy for the Last Termination in the North Atlantic region based on the Greenland ice-core record: a proposal by the INTIMATE group. Journal of Quaternary Science, 13(4): 283-292.

Bozarth, S.R., 1992. Classification of opal phytoliths formed in selected dicotyledons native to the Great Plains. In: G. Rapp Jr. and S.C. Mulholland (Editors), Phytolith Systematics: Emerging Issues. Plenum Press, New York, pp. 193-214.

Bozarth, S.R., 1998. Paleoenvironmental Reconstruction of the Sargent Site, Southwestern Nebraska – A Fossil Biosilicate Analysis, Abstracts – Institute for Tertiary-Quaternary Studies.

Bozarth, S.R., 2008. Procedure for Extraction of Opal Phytoliths from Sediment, unpublished manuscript.

Bremond, L., Alexandre, A., Peyron, O. and Guiot, J., 2005. Grass water stress estimated from phytoliths in West Africa. Journal of Biogeography, 32(2): 311-327.

Brown, D.A., 1984. Prospects and limits of a phytolith key for grasses in the central United States. Journal of Archaeological Science, 11: 345-368.

Cordova, C.E., Johnson, W.C., Mandel, R.D. and Palmer, M.W., 2011. Late Quaternary environmental change inferred from phytoliths and other soil-related proxies: Case studies from the central and southern Great Plains, USA. Catena.

Delhon, C., 2007. Phytolith and pedoanthracological analysis of 'off-site' Holocene sequences from Mondragon (middle Rhone Valley, south of France). In: M. Madella and D. Zurro (Editors), Plants, people and places: recent studies in phytolith analysis. Oxbow Books, pp. 175-188.

Edwards, E.J., and Still, C.J., 2008. Climate, phylogeny and the ecological distribution of C4 grasses. Ecology Letters, 11:226-276.

Feggestad, A.J., Jacobs, P.M., Miao, X.D., and Mason, J.A., 2004. Stable carbon isotope record of Holocene environmental change in the central Great Plains. Physical Geography 25, 170-190.

Frakes, L.A., and Jianzhoung, S., 1994. A carbon isotope record of the upper Chinese loess sequence: Estimates of plant types during stadials and interstadials. Palaeogeography, Palaeoclimatology, Palaeoecology, 108(1-2): 183-189.

Fredlund, G.G., Johnson, W.C. and Dort Jr., W., 1985. A Preliminary Analysis of Opal Phytoliths from the Eustis Ash Pit, Frontier County, Nebraska. Institute for Tertiary-Quaternary Studies - TER-QUA Symposium Series(1): 147-162.

Fredlund, G.G. and Tieszen, L.T., 1994. Modern Phytolith Assemblages from the North American Great Plains. Journal of Biogeography, 21(3): 321-335.

Fredlund, G.G. and Tieszen, L.L., 1997. Calibrating grass phytolith assemblages in climatic terms: Application to late Pleistocene assemblages from Kansas and Nebraska. Palaeogeography, Palaeoclimatology, Palaeoecology, 136(1–4): 199-211.

Garnier, A., Neumann, K., Eichhorn, B., and Lespez, L., 2013. Phytolith taphonomy in the middle- to late-Holocene fluvial sediments of Ounjugou (Mali, West Africa). The Holocene, 23(3): 416-431.

Grimm, E.C., 1987. CONISS: a Fortran 77 program for stratigraphically constrained cluster analysis by the method of incremental sum of squares. Computers and Geosciences, 13: 13-35.

Grimm, E.C., 2011. Tilia. Illinois State Museum Research and Collections Center, Springfield, IL.

Holliday, V.T., Meltzer, D.J., and Mandel, R., 2011. Stratigraphy of the Younger Dryas Chronozone and paleoenvironmental implications: Central and Southern Great Plains. Quaternary International, 242(2): 520-533.

HPRCC, 2013. Historical Data Summaries. High Plains Regional Climate Center http://www.hprcc.unl.edu/data/historical/.

Jacobs, P.M. and Mason, J.A., 2004. Paleopedology of soils in thick Holocene loess, Nebraska, USA. Revista Mexicana de Ciencias Geologicas, 21(1): 54-70.

Johnson, W.C. and Willey, K.L., 2000. Isotopic and rock magnetic expression of environmental change at the Pleistocene-Holocene transition in the central Great Plains. Quaternary International(67): 89-106.

Kollmorgen, H.L., 1963. Isopachous Map and Study on Thickness of Peorian Loess in Nebraska. Soil Sci Soc Am J, 27(4): 445-448.

Kurmann, M.H., 1985. An Opal Phytolith and Palynomorph Study of Extant and Fossil Soils in Kansas (USA). Palaeogeography Palaeoclimatology Palaeoecology, 49(3-4): 217-235.

Liu, W., Ning, Y., An, Z., Wu, Z., Lu, H., and Cao, Y., 2005. Carbon isotopic composition of modern soil and paleosol as a response to vegetation change on the Chinese Loess Plateau. Science in China Series D: Earth Sciences, 48(1): 93-99.

Lu, H., Wu, N., Yang, X., Jiang, H., Liu, K., Liu, T., 2006. Phytoliths as quantitative indicators for the reconstruction of past environmental conditions in China I: phytolith-based transfer functions. Quaternary Science Reviews, 25(9-10): 945-959.

Magill, C.R, Ashley, G.M., and Freeman, K.H., 2013. Ecosystem variability and early human habitats in eastern Africa. Proceedings of the National Academy of Sciences of the United States of America, 110: 1167-1174.

Mason, J.A., 1998. Relative rates of Peoria Loess accumulation and pedogenic processes: Implications for paleoclimatic inference. Quaternary International, 51/52: 169-174.

Mason, J.A., 2001. Transport Direction of Peoria Loess in Nebraska and Implications for Loess Sources on the Central Great Plains. Quaternary Research, (56): 79-86.

Mason, J.A., Jacobs, P.M., Hanson, P.R., Miao, X., and Goble, R.J., 2003. Sources and paleoclimatic significance of Holocene Bignell Loess, central Great Plains, USA. Quaternary Research, (60): 330-339.

Mason, J.A., Miao, X., Hanson, P.R., Johnson, W.C., Jacobs, P.M., and Goble, R.J., 2008. Loess record of the Pleistocene-Holocene transition on the northern and central Great Plains, USA. Quaternary Science Review, 27: 1772-1783.

Miao, X., Mason, J.A., Goble, R. J., and Hanson, P.R., 2005. Loess record of dry climate and aeolian activity in the early- to mid-Holocene, central Great Plains, North America. The Holocene, 15(3): 339-346.

Miao, X., Mason, J.A., Johnson, W.C. and Wand, H., 2007. High-resolution proxy record of Holocene climate from a loess section in Southwestern Nebraska, USA. Palaeogeography, Palaeoclimatology, Palaeoecology, (245): 368-381.

Muhs, D.R., Bettis, E.A., Aleinikoff, J.N., McGeehin, J.P., Beann, J., Skipp, G., Marshall, B.D., Roberts, H.M., Johnson, W.C., and Benton, R., 2008. Origin and paleoclimatic significance of late Quaternary loess in Nebraska: Evidence from stratigraphy, chronology, sedimentology, and geochemistry. Geological Society of America Bulletin, 120(11-12): 1378-1407.

Mulholland, S.C. and Rapp Jr., G., 1992a. Phytolith Systematics: An Introduction. In: G. Rapp Jr. and S.C. Mulholland (Editors), Phytolith Systematics: Emerging Issues. Plenum Press, New York, pp. 1-13.

Mulholland, S.C. and Rapp Jr., G., 1992b. A Morphological Classification of Grass Silica-Bodies. In: G. Rapp Jr. and S.C. Mulholland (Editors), Phytolith Systematics: Emerging Issues. Plenum Press, New York, pp. 65-90.

Nordt, L., von Fischer, J., Tieszen, L., 2007. Late Quaternary temperature record from buried soils of the North American Great Plains. Geology (35): 159-162.

Orombelli, G., Maggi, V. and Delmonte, B., 2010. Quaternary stratigraphy and ice cores. Quaternary International, 219(1-2): 55-65.

Piperno, D.R., 1988. Phytolith Analysis: An Archaeological and Geological Perspective. Academic Press, Inc., San Diego.

Piperno, D.R., 2006. Phytoliths: A Comprehensive Guide for Archaeologists and Paleoecologists. AltaMira Press, Lanham, MD, 238 pp.

Pohl, R.W., 1954. How to Know the Grasses (Pictured Key Nature Series). W. C. Brown Company Dubuque, Iowa, 200 pp.

Roberts, P., Lee-Thorp, J.A., Mitchell, P.J., and Arthur, C., 2013. Stable carbon isotopic evidence for climate change across the late Pleistocene to early Holocene from Lesotho, southern Africa. Journal of Quaternary Science, 28(4): 360-369.

Sangster, A.G. and Parry, D.W., 1969. Some Factors in Relation to Bulliform Cell Silicification in the Grass Leaf. Annals of Botany, 33(2): 315-323.

Schultz, C.B. and Stout, T.M., 1948. Pleistocene mammals and terraces in the Great Plains. Geological Society of America Bulletin, 59: 541-630.

Thorp, J. and Smith, H.T.U., 1952. Pleistocene eolian deposits of the United States, Alaska, and parts of Canada. Washington National Research Council, Geological Society of America, New York.

Cerling, T.E., 1984. The stable isotopic composition of modern soil carbonate and its relationship to climate. Earth and Planetary Science Letters, 71(2): 229-240.

Twiss, P.C., 1983. Dust Deposition and Opal Phytoliths in the Great Plains. Transactions of the Nebraska Academy of Sciences(XI-Special Issue): 73-82.

Twiss, P.C., 1987. Grass-opal phytoliths as climatic indicators of the Great Plains Pleistocene. In: W.C. Johnson (Editor), Quaternary environments of Kansas. Kansas Geological Survey Guidebook Series 5. Kansas Geological Survey, Lawrence, pp. 179-188.

Twiss, P.C., Suess, E. and Smith, R.M., 1969. Morphological Classification of Grass Phytoliths. Soil Sci Soc Am Proc, 33: 109-115.

Wilding, L.P. and Drees, L.R., 1973. Scanning electron microscopy of opaque opaline forms isolated from forest soils in Ohio. Soil Science Society of America, Proceedings, 37: 674-650.

Wang, G., Feng, X., Han, J., Zhou, L., Tan, W., and Su, F., 2008. Paleovegetation reconstruction using Delta 13C of Soil Organic Matter. Biogeosciences, (5): 1325-1337.

Woodburn, T.L., Hasiotis, S. T., and Johnson, W. C., in preparation. Assessing bioturbation in the Brady Soil using micromorphology and phytolith analysis.

Wynn, J.G., 2000. Paleosols, stable carbon isotopes, and paleoenvironmental interpretation of Kanapoi, Northern Kenya. Journal of Human Evolution, 39(4): 411-432.

Zhou, B., Shen, C., Zheng, H., Zhou, M., and Sun, Y., 2009. Vegetation evolution on the central Chinese Loess Plateau since late Quaternary evidenced by elemental carbon isotopic composition. Chinese Science Bulletin, 54(12): 2082-2089.

Zielinski, G.A. and Mershon, G.R., 1997. Paleoenvironmental implications of the insoluble microparticle record in the GISP2 (Greenland) ice core during the rapidly changing climate of the Pleistocene-Holocene transition. Geological Society of America Bulletin 109(5): 547-559.

Figures

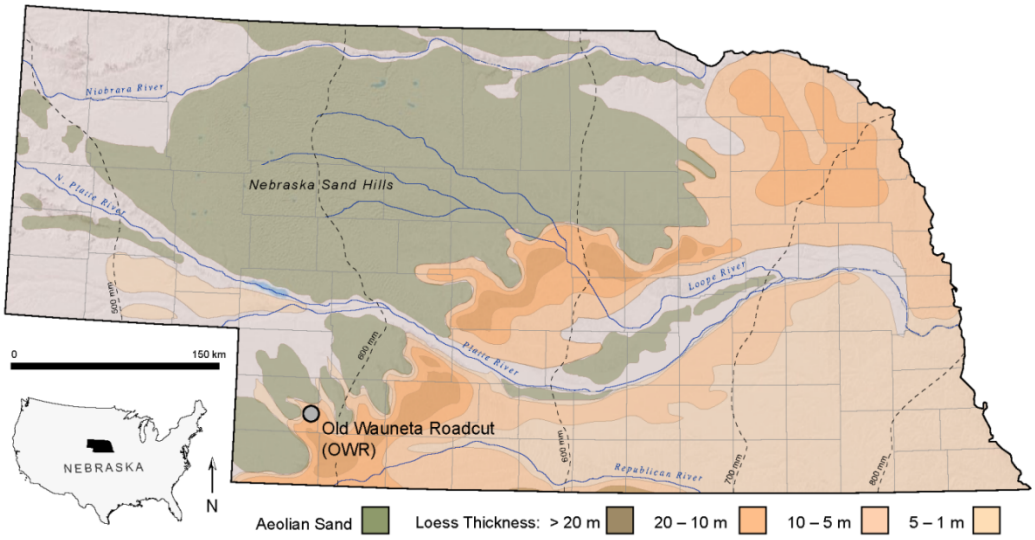

Fig. 1 – Old Wauneta Roadcut location in southwestern Nebraska. Aeolian sand and loess distribution and thickness (modified from Bettis III et al., 2003).

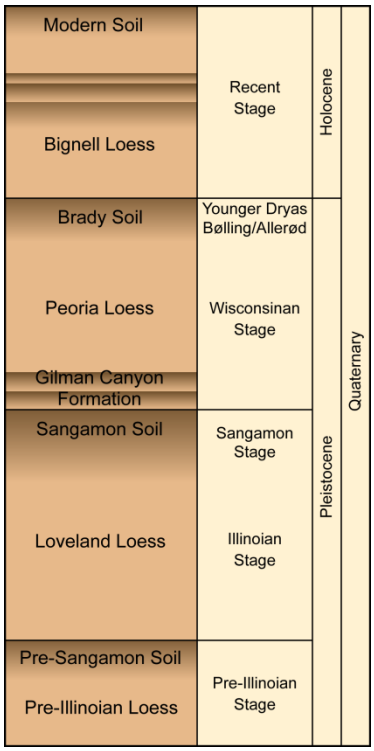

Fig. 2 – Regional late Quaternary loess/paleosol stratigraphy (modified from Baars and Maples, 1998, and Johnson and Willey, 2000).

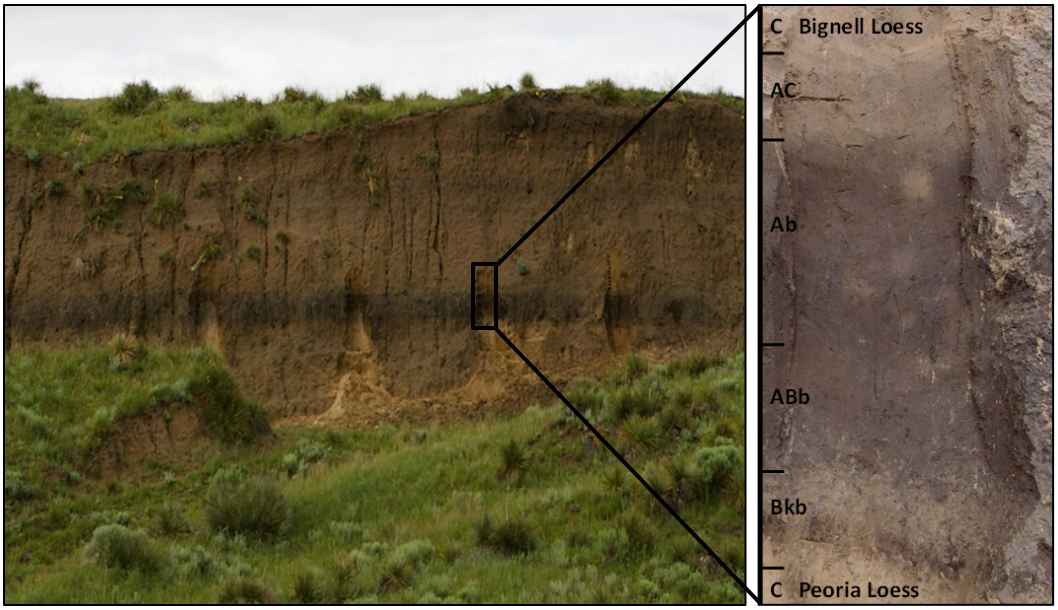

Fig. 3 – Example of a strategraphic profile of the Brady Soil from the Old Wauneta Roadcut exposure characterized by thick, cumulic, organic-rich horizons spaning the Pleistocene-Holocene transition.

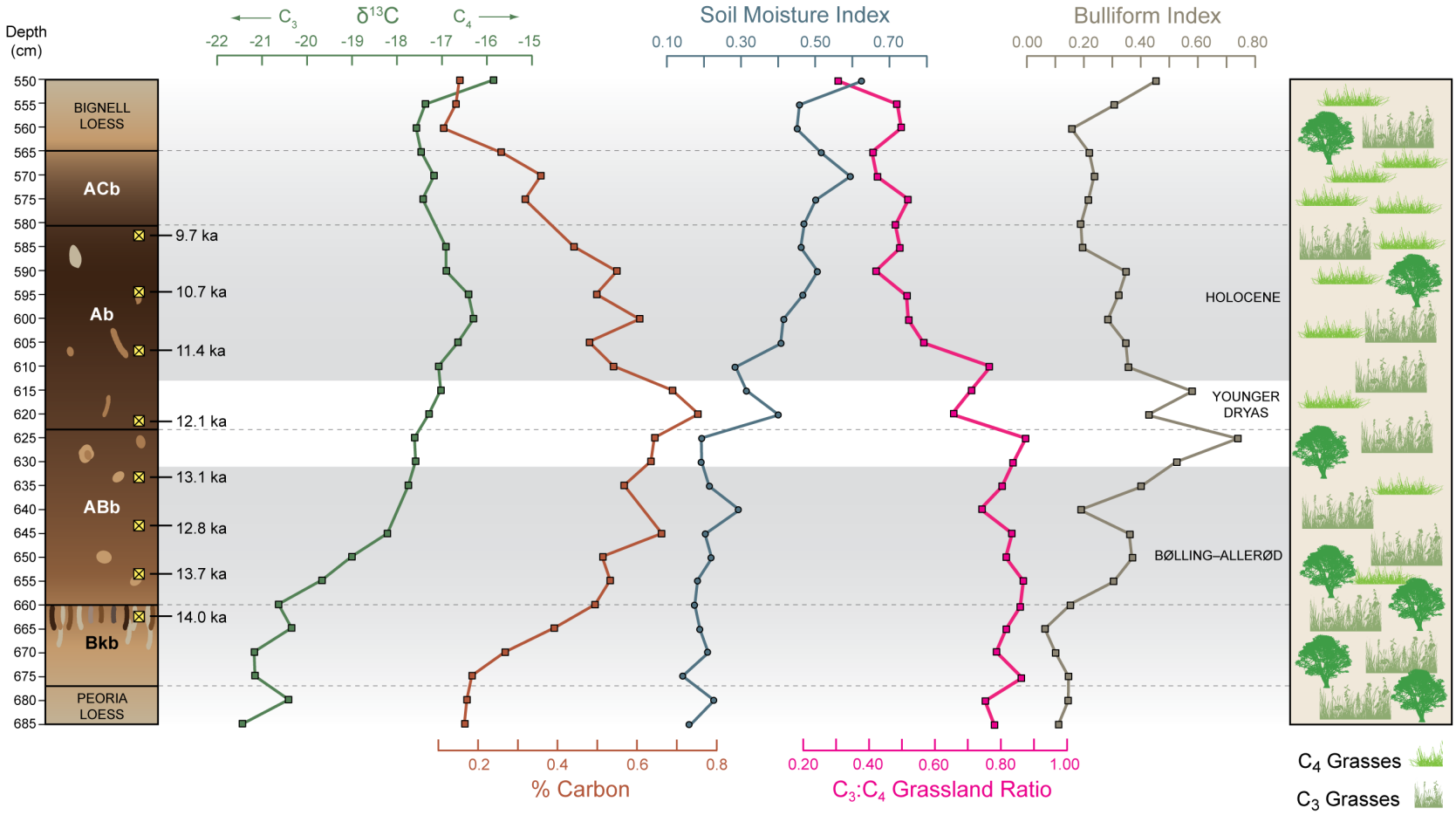
Depth (cm)
δ13C
C3
C4
-22 -21 -20 -19 -18 -17 -16 -15
Soil Moisture Index
0.10 0.30 0.50 0.70
Bulliform Index
0.00 0.20 0.40 0.60 0.80
550 555 560 565 570 575 580 585 590 595 600 605 610 615 620 625 630 635 640 645 650 655 660 665 670 675 680 685
BIGNELL LOESS
ACb
Ab
ABb
Bkb
PEORIA LOESS
9.7 ka
10.7 ka
11.4 ka
12.1 ka
13.1 ka
12.8 ka
13.7 ka
14.0 ka
HOLOCENE
YOUNGER DRYAS
BØLLING–ALLERØD
0.2 0.4 0.6 0.8
% Carbon
0.20 0.40 0.60 0.80 1.00
C3:C4 Grassland Ratio
C4 Grasses
C3 Grasses

Fig. 4 – Stable carbon isotope ($\delta^{13}C$), percent carbon (% C), and climate index trends for the Brady Soil. Values are shown with respect to the Brady Soil stratigraphy and **c**alibrated radiocarbon ages (Mason et al., 2008). C_3:C_4 Grassland Ratio values nearing zero are C_4-dominant grasslands indicating warmer temperatures, while values nearing 1 are C_3-dominant grasslands indicating cooler temperatures. Soil Moisture Index values nearing zero indicate more mesic conditions with values nearing 1 indicate increasing aridity. Bulliform index values nearing zero equates to low water stress environments with increasing water stress and evapotranspiration occurring nearing a value of 1. The right column displays the general distribution of deciduous trees, C_3 grasses, and C_4 grasses from the open woodland/savannah conditions in the late Pleistocene to the grass-dominated early Holocene.

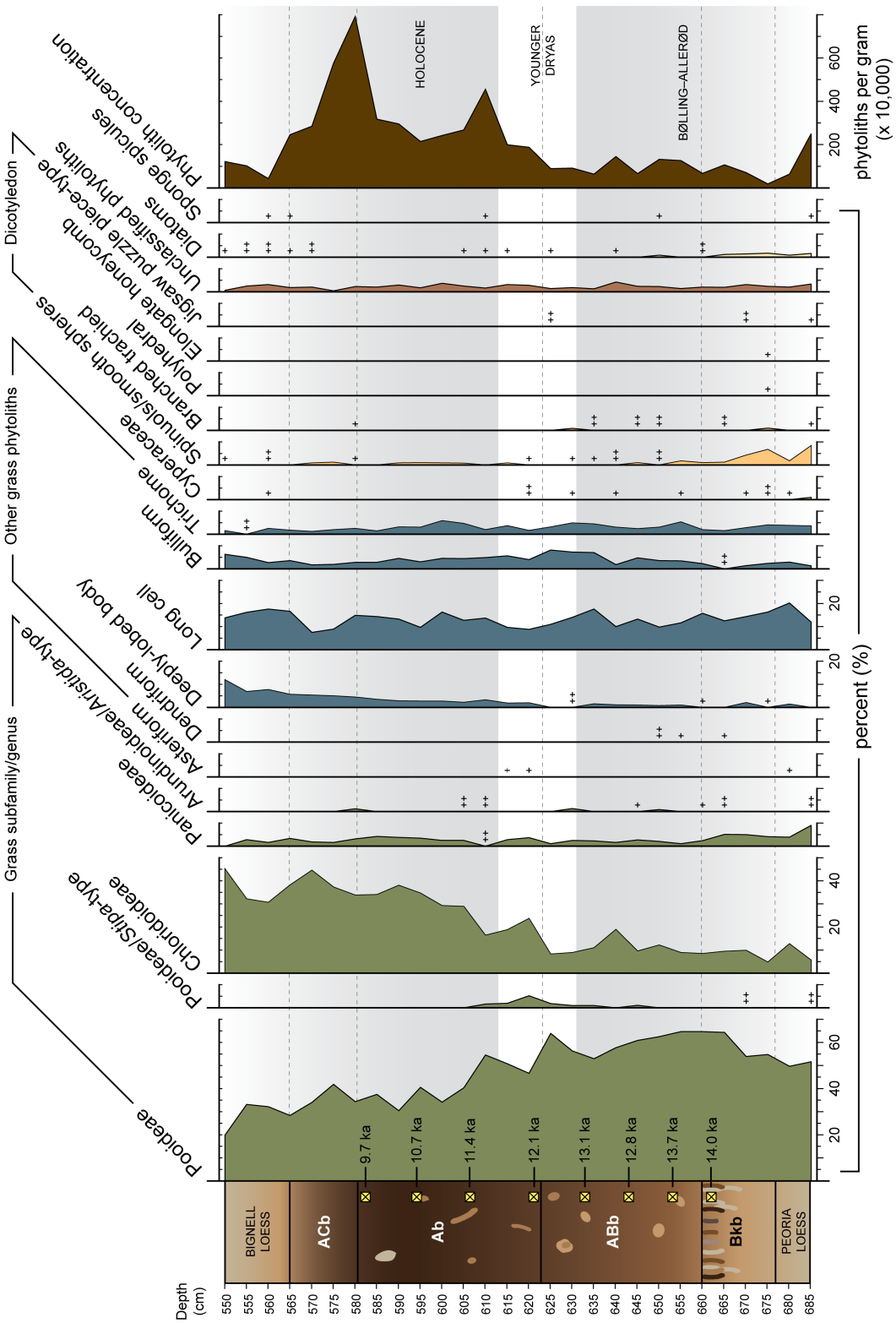
Depth (cm)
BIGNELL LOESS
ACb
Ab
ABb
Bkb
PEORIA LOESS
9.7 ka
10.7 ka
11.4 ka
12.1 ka
13.1 ka
12.8 ka
13.7 ka
14.0 ka
HOLOCENE
YOUNGER DRYAS
BØLLING–ALLERØD
phytoliths per gram (x 10,000)
percent (%)
Grass subfamily/genus
Other grass phytoliths
Dicotyledon
Pooideae
Pooideae/Stipa-type
Chloridoideae
Panicoideae
Arundinoideae/Aristida-type
Asterifiorm
Dendriform
Deeply-lobed body
Long cell
Bulliform
Trichome
Cyperaceae
Spinulos/smooth spheres
Branched/smooth spheres
Polyhedral
Elongate honeycomb
Jigsaw puzzle piece-type
Unclassified phytoliths
Diatoms
Sponge spicules
Phytolith concentration

Fig. 5 – Biosilicate frequencies and phytolith concentrations shown with respect to the Brady Soil stratigraphy. Shaded zones indicate distinct vegetation assemblages that correlate to the North Atlantic cronosequence.

Chapter 4. Conclusions

Results from this dissertation go beyond previous paleoenvironmental descriptions of the Brady Soil by defining vegetation assemblages and quantifying plant community changes through the Pleistocene-Holocene transition. Given the lack of natural lakes in the Great Plains region necessary for adequate pollen record preservation, phytoliths are the only viable source from which detailed vegetation history may be obtained. Phytolith analysis is more time consuming than the commonly-employed $\delta^{13}C$ analysis utilized to detect shifts in C_3 and C_4 plant dominance, but is essential for enhanced climate interpretations. Climate indices produced from phytolith frequencies helped define changes in temperature, moisture, and evapotranspiration rates.

Trends in the C_3 and C_4 vegetation signal documented with phytolith frequencies correlate well with stable carbon isotope data ($\delta^{13}C$). Through phytolith analysis, the late-Pleistocene Bølling-Allerød was characterized as savannah to open woodland with a cool, mesic climate by the presence of deciduous trees, in addition to Pooideae (C_3) grass dominance. A comparison of aridity and soil moisture indices, along with low frequencies of Chloridoideae (C_4) grass, indicates very little seasonal variability during the B-A.

Stipa-type Pooideae phytoliths signal climate change within the Younger Dryas time period, previously undetected by $\delta^{13}C$ analysis of the Brady Soil. The *Stipa* genus is a cool-season grass that grows in dry conditions indicating a transition away from mesic conditions. Additionally, the decrease in long cell phytoliths and increase in evapotranspiration detected by the Bulliform Index provides corroboration for rapid warming and drying. Mixed-grass praires of the early Holocene displays a continued warming trend, yet evapotranspiration decreases due to more efficient use of moisture by the added warm-season Chloridoideae grasses. A separation of the aridity and soil

moisture indices during this time indicates a change to seasonal variations in temperature and moisture.

Accuracy of data obtained from the Brady Soil was also a priority of this research. Due to floral and faunal bioturbation, original sediment deposition and soil horizonation have been altered. Detailed examination of bioturbation using macro- and micro-morphology and phytolith distributions has been used to determine the extent of mixing and to evaluate age and proxy data precision. Two major trace makers were identified based on comparisons with modern analogues. Cicada (Cicadidae) nymphs or similar invertebrates produced distinctive meniscate backfilled burrows throughout the soil profile, but occur in a high concentration in the upper Bkb horizon. These invertebrates create local (diffusive) mixing by actively moving sediment from one location to another. The presence of cicada in this environment, and in highest concentrations within the Bkb horizon, substantiates the phytolith evidence for woody vegetation existence on the upland loess plateaus during the B-A. Domichnia produced by rodents, such as prairie dogs (*Cynomys* sp.) or ground squirrel (*Spermophilus* sp.), are also distributed through the Brady Soil, creating deep, non-local (advective) mixing, mostly containing passive fill from surface sediment falling into open burrows and chambers. Instances of burrow systems containing passive fill represent post-soil formation bioturbation events.

Through the use of L*a*b color, particle size distribution, and phytolith distributions, sediment was tracked to their profile source level. Micromorphology of rodent burrow samples showed additional localized mixing of the infill material, however, non-local mixing events were easily definable in the soil profile. Local mixing events have been found to be prevalent in the Brady Soil and need to be accounted for in sampling strategies. A 5-cm sampling resolution has been proven sufficient for relatively

high-resolution proxy analysis within the Brady Soil, while higher-resolution studies may show greater variation in proxy signals due to localized bioturbation.

Appendices

Appendix A: Procedure for Isolation of Opal Phytoliths from Sediment

Adapted from Steven R. Bozarth
University of Kansas Palynology Laboratory
Department of Geography
2008, Updated 9/6/13

Sample Preparation

Dry loose sediment in paper bag or desiccator.

Always use distilled or reverse osmosis water.

1. For loose sediment, shake sample through a 2 mm (2000μm) sieve or thoroughly mix in plastic bag. If sample is in block form (such as clayey fields at Blue Creek), then take sub-sample vertically. It is most efficient to process eight samples at one time.

2. Place 10 grams of sediment[1] in a 400 ml beaker for most contexts in sites in karst topography (20 g may be too much, see 03.10.30.5-7). Use 5 gram samples for the Great Plains and American Southwest unless very sandy.

Introduction of spike spores and removal of carbonates

3. Add **1-10** Lycopodium tablets (if working in a grass land, then add 10). Add 25 ml 10% hydrochloric acid (HCL) (2 parts water to 1 part concentrated HCL). Wait for tablets to dissolve. If strong reaction occurs due to carbonates, wait 5-10 minutes and add more HCL. Repeat until there is no reaction. If strong reaction occurred, then it may necessary to wash off side of beaker with jet of H_20.

4. Transfer sample to a 250 ml centrifuge bottle.

5. Add water to make the bottle 3/4 full, balance, shake, and centrifuge in an IEC floor-model centrifuge at setting 25 for 5 minutes. Decant slowly or siphon if sample is sandy. If plant

material or foam adheres to inside of bottle, twist bottle while decanting to wash it out. Watch to determine if sediment starts to run out, if so, centrifuge again and siphon off supernatant. **Repeat once**. This will wash out the HCL.

Removal of colloidal organics, clays, and very fine silts

6. Add 100 ml (150 ml if karst) sodium pyrophosphate solution (71.4 g sodium pyrophosphate in 1600 ml water). Shake sample and wash off inside of bottle with fine jet of distilled H_20 if necessary. Place sample in ultrasonic bath for 15 minutes. Let set overnight if clayey!

7. Add water to make the bottle 3/4 full, balance, shake, and centrifuge at setting 18 for 5 minutes. Pour supernatant through 5 μm nitex filter using an aspirator. This allows clays and fine silts to pass through but prevents discarding most phytoliths. Stop decanting if nitex stops up. Squirt nitex with jet of water. Wash filter off over beaker. Repeat this step at slower speeds (e.g., 17, 16, 15, 14) for five minutes as long as most of supernatant can be decanted and until supernatant is no longer cloudy. It may be necessary to repeat step 6 after decanting 2-3 times if sample is very clayey. **Transfer contents of beaker back into centrifuge bottle after next to last centrifugation.** After last decantation, add water, shake, and pour through **125 μm sieve** placed over 400 ml beaker if plant material or coarse sand is present. Transfer to bottle.

8. Add water to make bottle ½ full, balance, shake, and centrifuge at setting 25 for 5 minutes. **Siphon** off most of supernatant (down to "ring" above base of bottle), being careful not to draw up any sediment. Repeat steps 6 and 7 if clay aggregates persist.

9. Transfer sample to 40 ml glass centrifuge tube (shake bottle and pour into beaker; add ca. 10 ml H_20 to bottle, shake and pour into beaker; swirl beaker and pour into tube) balance, and centrifuge at setting 25 for 5 minutes. Don't add past frosted area to avoid breakage. **Decant** or siphon out supernatant.

Oxidation for American Southwest or Great Plains (<u>usually not necessary</u>)

For organic rich samples add 20 ml H_20_2. It may be necessary to oxidize in hot water bath overnight to remove organics. 30% H_20_2 at room temperature will not oxidize pollen or *Lycopodium* spores. There may some yellowing of *Lycopodium* spores Note: oxidation of Arizona sediment samples with Schulze solution[2] in a hot water bath at setting of 7 apparently causes certain minerals such as mica to become artificially "light".

Oxidation for karst topography (usually not necessary)

Add 5 ml H_20_2 (**Caution, strong reaction may occur)** If strong reaction occurs (typical of samples from Nakbe', reservoir at La Milpa, and Chunchucmil), it may be necessary to transfer sample back into beaker to avoid "foaming over". Repeat after 15 minutes until ca. 25 ml of H_20_2 have been added (up to 2nd level on tube rack). Place tube in warm water bath overnight at **setting 4** in fume hood to remove organics.

Add water to dilute H_20_2 and reduce sediment in suspension, balance and centrifuge at setting 25 for 5 minutes. Siphon or decant supernatant into drain with water running.

Add ca. 10 ml water, stir with vortex mixer, add another 20 ml water, balance, and centrifuge at setting 25 for 5 minutes and decant. Repeat.

Wash into 50 ml round-bottom centrifuge tube, add additional water if needed, balance, and centrifuge at setting 25 for 5 minutes and decant (pipette if sediment is sandy). Don't need to decant all of supernatant due to use of HCL in step 14.

Heavy liquid flotation and centrifugation

10. Add 20 ml $ZnBr_2$ (sp. gr. 2.32) to sample, stir on vortex mixer using rubber stopper in tube, and centrifuge at setting **25** for one hour[3]. Decant into a 50 ml centrifuge tube.

Dilution of sample

11. Add 30 ml water to 50 ml centrifuge tube, balance, **shake**, and centrifuge at setting 25 for 10 minutes. Phytoliths will sediment to bottom of tube. Decant dilute heavy liquid into bottle for recycling. If may be necessary to wash isolates from clayey samples e.g., BC fields, through nitex to remove any remaining clay to avoid clumping of final isolate. Note: floating a 2nd time rarely significantly increases the isolate purity. **Heat TBA**

Washing and dehydration of isolate

12. Add ca. 3 ml water, stir with vortex mixer, and pour into 12 ml centrifuge tube. Repeat as necessary to insure complete transfer of isolate. Balance and centrifuge at moderate speed (4-5) on tabletop centrifuge for 5 minutes, decant, and blot tube with a Kimwipe.

13. Add small amount of **warm** TBA, stir with vortex mixer, and decant into 1 dram glass vial. Repeat until all of isolate is transfered. Balance and centrifuge at moderate speed for 5 minutes.

Isolate storage

14. Remove most of supernatant by suction pipetting. Be careful to keep pipette above phytoliths. Set the vial on a slide warmer (setting 5) with the cap ajar to evaporate residual TBA.

Note: [1] 5 grams dry sediment = 7.85 grams wet (decanted after centrifugation). 1.57 g wet = 1 g dry

[2] Schulze solution is made by adding three parts concentrated nitric acid (HNO_3) to one part saturated potassium chlorate ($KCLO_3$), which is made by adding 7.1 g dry powdered $KCLO_3$ to 100 ml water.

[3] Water present in the pellet will slightly dilute the $ZnBr_2$. Using $ZnBr_2$ mixed to 2.32 allows for this dilution without going below 2.3

Add 180 ml R. O. water to one $ZnBr_2$ bottle (500 g) to make 2.3 specific gravity.

Add 170 ml R. O. water to one $ZnBr_2$ bottle (500 g) to make 2.32 specific gravity.

Appendix B: Phytolith Frequencies

Name	550 cmbs	555 cmbs	560 cmbs	565 cmbs	570 cmbs
Pooideae	63	106	104	94	113
Pooideae/*Stipa*-type	0	0	0	0	0
Chloridoideae	143	103	99	126	148
Panicoideae	0	9	5	11	6
Arundinoideae/*Aristida*-type	0	0	0	0	0
Asteriform	0	0	0	0	0
Dendriform	0	0	0	0	0
Deeply-lobed body	38	22	25	19	18
Long cell	44	52	57	55	25
Bulliform	20	16	9	12	6
Trichome	5	2	8	6	4
Cyperaceae	0	0	1	0	0
Spinulos/smooth Spheres	1	0	2	0	3
Branched trachied	0	0	0	0	0
Polyhedral	0	0	0	0	0
Elongate honeycomb	0	0	0	0	0
Jigsaw puzzle piece-type	0	0	0	0	0
Unclassified phytoliths	2	8	10	6	7
Algal statospore	0	0	0	0	0
Diatoms	1	2	2	1	2
Sponge spicules	0	0	1	1	0
Phytolith Concentration	1216355.8	1019410.3	423692.4	2460389.2	2847487.4
Charred phytoliths	1	2	0	0	15
Charcoal 20-80 µm	0	1	2	2	4

Name	575 cmbs	580 cmbs	585 cmbs	590 cmbs	595 cmbs
Pooideae	108	122	107	105	117
Pooideae/*Stipa*-type	0	0	0	0	0
Chloridoideae	96	120	97	131	100
Panicoideae	4	11	12	13	10
Arundinoideae/*Aristida*-type	0	4	0	0	0
Asteriform	0	0	0	0	0
Dendriform	0	0	0	0	0
Deeply-lobed body	13	16	10	10	8
Long cell	23	53	41	46	28
Bulliform	5	10	8	16	9
Trichome	5	9	4	11	9
Cyperaceae	0	0	0	0	0
Spinulos/smooth Spheres	3	1	0	3	3
Branched trachied	0	1	0	0	0
Polyhedral	0	0	0	0	0
Elongate honeycomb	0	0	0	0	0
Jigsaw puzzle piece-type	0	0	0	0	0
Unclassified phytoliths	1	8	6	10	5
Algal statospore	0	0	0	0	0
Diatoms	0	0	0	0	0
Sponge spicules	0	0	0	0	0
Phytolith Concentration	5753296.8	7916358	3177693	2958985.4	2148194.8
Charred phytoliths	2	0	1	2	0
Charcoal 20-80 µm	0	0	1	2	0

Name	600 cmbs	605 cmbs	610 cmbs	615 cmbs	620 cmbs
Pooideae	111	145	167	162	116
Pooideae/*Stipa*-type	0	0	5	6	13
Chloridoideae	95	104	50	60	59
Panicoideae	8	9	2	9	9
Arundinoideae/*Aristida*-type	0	2	2	0	0
Asteriform	0	0	0	1	1
Dendriform	0	0	0	0	0
Deeply-lobed body	9	8	10	6	5
Long cell	53	46	42	31	22
Bulliform	15	16	15	18	10
Trichome	19	17	6	12	4
Cyperaceae	0	0	0	0	2
Spinulos/smooth Spheres	3	3	0	3	1
Branched trachied	0	0	0	0	0
Polyhedral	0	0	0	0	0
Elongate honeycomb	0	0	0	0	0
Jigsaw puzzle piece-type	0	0	0	0	0
Unclassified phytoliths	12	9	5	10	7
Algal statospore	0	0	0	0	0
Diatoms	0	1	1	1	0
Sponge spicules	0	0	1	0	0
Phytolith Concentration	2415790	2675952	4549118.4	1995153.6	1880510.8
Charred phytoliths	2	0	0	2	1
Charcoal 20-80 µm	4	0	1	0	0

Name	625 cmbs	630 cmbs	635 cmbs	640 cmbs	645 cmbs
Pooideae	179	184	165	150	179
Pooideae/*Stipa*-type	5	3	3	0	3
Chloridoideae	23	29	34	49	28
Panicoideae	3	8	7	4	8
Arundinoideae/*Aristida*-type	0	4	0	0	1
Asteriform	0	0	0	0	0
Dendriform	0	0	0	0	0
Deeply-lobed body	0	2	5	3	3
Long cell	31	46	55	26	39
Bulliform	23	24	22	5	14
Trichome	9	16	14	8	7
Cyperaceae	0	1	0	1	0
Spinulos/smooth Spheres	0	1	1	2	3
Branched trachied	0	3	2	0	2
Polyhedral	0	0	0	0	0
Elongate honeycomb	0	0	0	0	0
Jigsaw puzzle piece-type	2	0	0	0	0
Unclassified phytoliths	4	6	4	11	7
Algal statospore	0	0	0	0	0
Diatoms	1	0	0	1	0
Sponge spicules	0	0	0	0	0
Phytolith Concentration	891984	911496.2	632497.8	1443699	655608.3
Charred phytoliths	4	3	4	2	0
Charcoal 20-80 µm	0	1	3	2	3

Appendix C: Environmental Index Calculations

Index	550 cmbs	555 cmbs	560 cmbs	565 cmbs	570 cmbs
Bulliform Index BI = bulliforms/longcells	0.45	0.31	0.16	0.22	0.24
Soil Moisture Index SMI = (chl+stipa)/ chl+st+po+pan+bull+long+tri)	0.52	0.36	0.35	0.41	0.49
C3:C4 Grassland Ratio C3:C4 = po+chl+pan)	0.31	0.49	0.50	0.41	0.42

Index	575 cmbs	580 cmbs	585 cmbs	590 cmbs	595 cmbs
Bulliform Index BI = bulliforms/longcells	0.22	0.19	0.20	0.35	0.32
Soil Moisture Index SMI = (chl+stipa)/ chl+st+po+pan+bull+long+tri)	0.40	0.37	0.36	0.41	0.37
C3:C4 Grassland Ratio C3:C4 = po+chl+pan)	0.52	0.48	0.50	0.42	0.52

Index	600 cmbs	605 cmbs	610 cmbs	615 cmbs	620 cmbs
Bulliform Index BI = bulliforms/longcells	0.28	0.35	0.36	0.58	0.45
Soil Moisture Index SMI = (chl+stipa)/ chl+st+po+pan+bull+long+tri)	0.32	0.31	0.19	0.22	0.31
C3:C4 Grassland Ratio C3:C4 = po+chl+pan)	0.52	0.56	0.77	0.71	0.65

Index	625 cmbs	630 cmbs	635 cmbs	640 cmbs	645 cmbs
Bulliform Index BI = bulliforms/longcells	0.74	0.28	0.21	0.08	0.29
Soil Moisture Index SMI = (chl+stipa)/ chl+st+po+pan+bull+long+tri)	0.10	0.10	0.12	0.20	0.11
C3:C4 Grassland Ratio C3:C4 = po+chl+pan)	0.88	0.83	0.80	0.74	0.83

Index	650 cmbs	655 cmbs	660 cmbs	665 cmbs	670 cmbs
Bulliform Index BI = bulliforms/longcells	0.16	0.12	0.28	0.54	0.10
Soil Moisture Index SMI = (chl+stipa)/ chl+st+po+pan+bull+long+tri)	0.13	0.09	0.09	0.10	0.12
C3:C4 Grassland Ratio C3:C4 = po+chl+pan)	0.82	0.87	0.86	0.82	0.79

Index	675 cmbs	680 cmbs	685 cmbs
Bulliform Index BI = bulliforms/longcells	0.15	0.14	0.11
Soil Moisture Index SMI = (chl+stipa)/ chl+st+po+pan+bull+long+tri)	0.06	0.14	0.08
C3:C4 Grassland Ratio C3:C4 = po+chl+pan)	0.86	0.75	0.78

Appendix D: Stable Carbon Isotope and Percent Carbon data

Depth	Amount (mg)	δ^{13}C VPDB	C%
550	12.796	–15.85	0.16
560	11.293	–17.37	0.15
655	6.624	-19.67	0.54
560	12.290	-17.57	0.12
565	11.359	-17.48	0.26
570	11.911	-17.16	0.36
575	6.172	-17.45	0.32
585	7.028	-16.91	0.45
590	6.775	-16.93	0.55
595	6.973	-16.43	0.50
600	7.261	-16.30	0.62
605	6.465	-16.65	0.48
610	7.220	-17.09	0.54
615	6.528	-17.03	0.69
620	5.531	-17.30	0.76
625	6.335	-17.63	0.65
630	5.411	-17.59	0.64
635	5.927	-17.76	0.57
645	6.431	-18.22	0.67
650	5.406	-19.02	0.52
660	6.157	-20.67	0.50
665	12.531	-20.34	0.40
670	13.712	-21.19	0.27
675	10.349	-21.17	0.19
680	11.073	-20.41	0.18
685	14.280	-21.45	0.17
690	10.754	-22.40	0.18
695	12.380	-21.40	0.14
700	11.007	-20.39	0.17
Burrows			
4	11.011	-17.36	0.31
5	6.243	-18.05	0.34
6	6.573	-17.03	0.39
7	12.644	-17.48	0.26
8	6.355	-17.30	0.47
9	12.828	-17.18	0.14

Appendix E: L*a*b* and Munsell color data

Dry:	L*(D65)	a*(D65)	b*(D65)	Munsell Hue	Munsell Value	Munsell Chroma
	54.16	5.51	17.18	0.1Y	5.31	2.77
	58.96	4.7	15.13	10.0YR	5.78	2.42
	59.89	5.01	16.14	10.0YR	5.88	2.59
	54.96	4.05	13.18	0.3Y	5.38	2.1
	51.44	3.59	10.85	10.0YR	5.02	1.77
	49.08	3.6	10.32	9.8YR	4.79	1.68
	47.13	3.42	9.5	9.7YR	4.6	1.54
	46.76	3.16	9.1	9.8YR	4.57	1.46
	45.94	3.16	9.02	9.8YR	4.49	1.44
	46.57	3.24	9.26	9.8YR	4.55	1.49
	44.68	2.94	8.26	9.8YR	4.36	1.31
	48.64	3.17	9.89	0.2Y	4.75	1.58
	47.44	3.28	10.04	0.2Y	4.64	1.6
	44.3	2.83	8.03	9.8YR	4.33	1.27
	42.57	2.8	7.88	9.8YR	4.16	1.24
	43.11	2.87	8.17	9.8YR	4.21	1.29
	43.88	3.02	8.48	9.8YR	4.29	1.34
	44.53	2.83	8.28	9.9YR	4.35	1.31
	48.58	2.59	7.36	9.7YR	4.74	1.19
	45.82	2.77	8.2	10.0YR	4.47	1.3
	46.57	3.07	9.08	10.0YR	4.55	1.45
	48.52	3.42	10.6	0.2Y	4.74	1.69
	50.07	3.72	11.28	0.1Y	4.89	1.82
	50.51	3.39	11.13	0.5Y	4.93	1.78
	55.33	3.99	13.9	0.6Y	5.42	2.19
	57.97	4.33	15.08	0.5Y	5.68	2.38
	59.72	4.53	15.92	0.4Y	5.86	2.51
	57.68	4.24	15.22	0.6Y	5.66	2.39
	57.16	4.63	17.15	0.8Y	5.61	2.68
	57.15	4.67	17.12	0.7Y	5.61	2.68
	56.08	4.59	16.81	0.8Y	5.5	2.63
	59.34	5.09	18.5	0.6Y	5.83	2.91
	58.74	5.22	18.86	0.6Y	5.77	2.97
	59.71	5.07	18.49	0.6Y	5.87	2.9
	60.18	5	18.36	0.6Y	5.91	2.88
	51.95	4.37	15.07	0.7Y	5.09	2.38
	42.39	3.87	11.1	10.0YR	4.15	1.74
	49.88	4.32	14.1	0.5Y	4.88	2.24
	48.64	4.07	13.25	0.5Y	4.76	2.09
	48.45	3.7	13.13	1.0Y	4.74	2.04
	45.75	3.81	11.94	0.4Y	4.48	1.87
	52.61	4.16	14.09	0.6Y	5.15	2.24
	42.45	3.52	11.37	0.6Y	4.16	1.75
	56.1	5	16.92	0.4Y	5.51	2.69
	53.95	4.04	14.7	0.8Y	5.28	2.3
	53.26	4.02	14.69	0.9Y	5.22	2.3

Moist	L*(D65)	a*(D65)	b*(D65)	Munsell Hue	Munsell Value	Munsell Chroma
	36.45	5.03	13.72	0.2Y	3.59	2.22
	45.52	3.42	9.54	9.9YR	4.45	1.52
	47.37	3.94	10.95	9.9YR	4.63	1.77
	44.62	3.13	8.4	9.7YR	4.36	1.35
	39.94	2.3	5.49	9.3YR	3.9	0.88
	38.49	2.57	6.27	9.4YR	3.76	1.01
	35.53	2.22	5.46	9.6YR	3.48	0.89
	33.32	2.14	5.66	0.1Y	3.26	0.92
	35.56	2.23	5.75	9.8YR	3.48	0.93
	38.36	2.22	5.61	9.6YR	3.75	0.9
	34.05	2.04	5.36	10.0YR	3.33	0.87
	36.84	2.12	5.46	9.8YR	3.6	0.87
	34.14	2.04	5.77	0.4Y	3.34	0.92
	33.03	1.89	5.06	0.2Y	3.23	0.82
	34.82	1.81	4.86	10.0YR	3.41	0.78
	34.27	1.83	4.96	0.1Y	3.35	0.8
	35.51	1.85	5.13	0.1Y	3.47	0.82
	35.47	1.87	4.97	10.0YR	3.47	0.8
	34.19	1.85	5.21	0.3Y	3.35	0.83
	34.79	1.83	4.98	0.1Y	3.4	0.8
	36.19	2.07	5.63	10.0YR	3.54	0.9
	33.82	2.66	7.49	0.4Y	3.32	1.21
	37.78	2.79	7.36	9.8YR	3.7	1.18
	40.69	2.69	7.73	10.0YR	3.98	1.2
	41.41	3.49	10.29	0.2Y	4.05	1.59
	45.12	3.85	11.4	0.2Y	4.42	1.8
	45.14	4.02	12.31	0.4Y	4.42	1.93
	44.92	3.45	10.29	0.3Y	4.39	1.62
	38.47	4.75	13.47	0.3Y	3.78	2.13
	38.33	5.21	15.73	0.7Y	3.78	2.47
	35.18	4.51	13.01	0.6Y	3.47	2.1
	41.69	5.86	17.82	0.6Y	4.11	2.77
	40.66	5.78	17.27	0.6Y	4	2.68
	41.31	5.84	17.25	0.5Y	4.07	2.69
	40.49	5.58	16.2	0.4Y	3.98	2.52
	40.05	5	15.78	0.7Y	3.94	2.43
	26.94	3.67	9.04	0.1Y	2.66	1.58
	32.97	4.41	12.41	0.5Y	3.25	2.04
	31.27	4.19	11.33	0.3Y	3.09	1.89
	30.66	3.07	8.54	0.7Y	3.02	1.42
	27.96	3.19	8.31	0.4Y	2.76	1.43
	34.42	4.41	12.75	0.5Y	3.39	2.06
	27.06	3.34	9.08	0.7Y	2.67	1.56
	39.48	5.46	15.83	0.4Y	3.89	2.49
	35.03	4.24	12.58	0.7Y	3.45	2.02
	34.04	4	12.12	0.8Y	3.35	1.95

Appendix F: Particle Size Analysis data

Depth (cmbs)	Clay <2 um	silt 2-63 um	Sand >63 um
550	3.09	57.67	39.24
555	3.07	55.48	41.46
560	2.95	51.46	45.58
565	3.13	59.94	36.93
570	3.44	65.70	30.87
575	3.21	61.79	35.00
580	3.08	62.85	34.07
585	3.07	64.58	32.35
590	3.16	71.16	25.68
595	3.12	69.56	27.32
600	2.90	66.84	30.26
605	2.85	66.49	30.66
610	2.97	63.78	33.25
615	2.73	65.26	32.01
620	2.80	65.41	31.79
625	2.62	64.73	32.66
630	2.66	63.05	34.28
635	2.68	64.14	33.19
640	2.79	63.98	33.23
645	2.73	62.94	34.33
650	2.74	63.38	33.88
655	3.12	62.55	34.33
660	3.21	65.41	31.39
665	3.16	64.35	32.49
670	3.14	62.47	34.39
675	3.16	63.56	33.28
680	2.63	58.13	39.23
685	3.23	63.72	33.05

burrows	Clay <2 um	silt 2-63 um	Sand >63 um
1	2.87	61.08	36.05
2	3.03	64.55	32.42
3	3.08	61.84	35.08
4	2.94	61.13	35.93
5	2.75	62.43	34.81
8	2.79	64.28	32.93
9	2.96	55.94	41.10
Chamber	2.89	61.12	35.99

Appendix G: Brady Soil Charcoal Counts and Magnetic Susceptibility

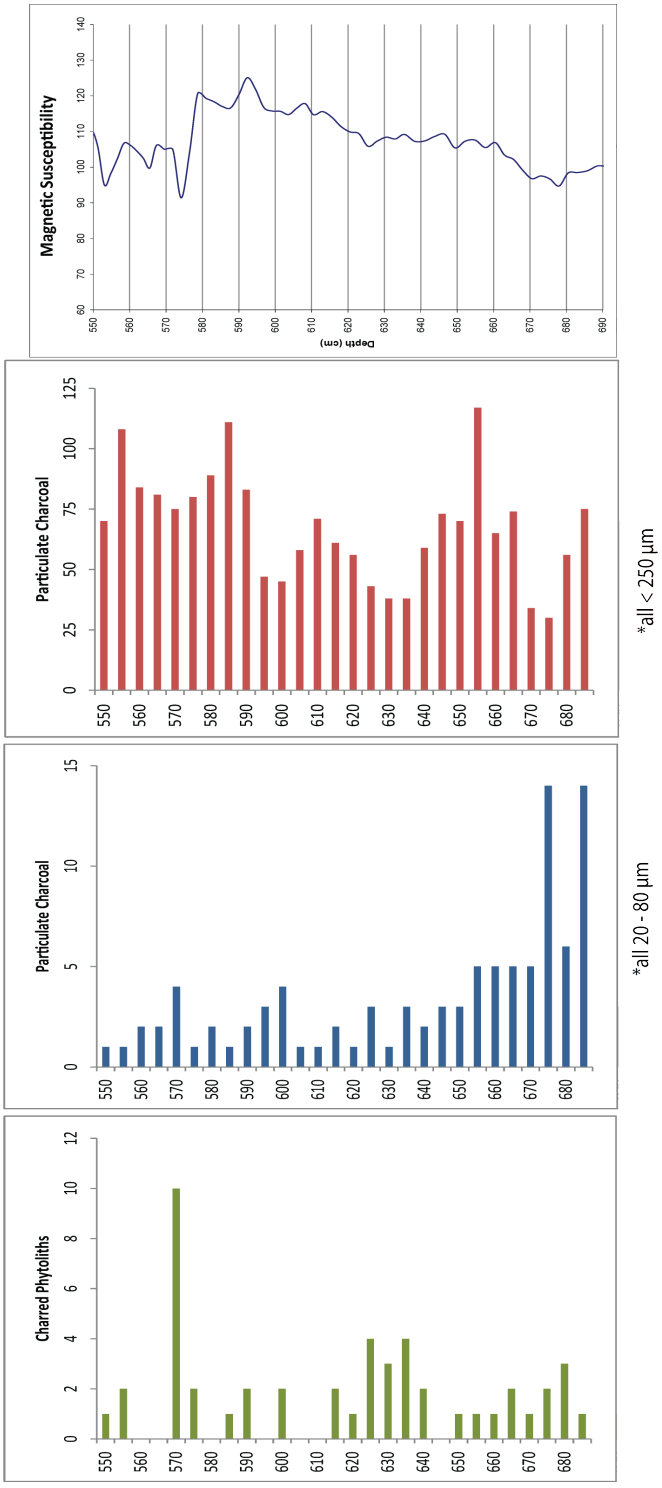

Charred phytoliths and particulate charcoal (20-80 μm) from phytolith slide counts by depth. Particulate charcoal from sieved and bleached sediment samples showing possible non-local charcoal source due to sizes under 250 μm; most charcoal particles have no structure or branching, are both irregular and geometric shapes. Most were blocky and black in color, with very few fibrous structures and brown coloring. Low frequency magnetic susceptibility analyzed from cube samples at the University of Kansas Soils and Geomorphology Laboratory.

Low frequency values for magnetic susceptibility:

Depth	Weight	Bkground	Raw LF	Adj. LF
708	17.39	0	115.4	115.35
705	14.52	0.1	84.8	84.7
702	15.9	0.1	103.7	103.6
700	15.72	0.1	99.8	99.7
697	15.56	0.1	96.2	96.05
694	16.62	0.2	111.5	111.3
691	14.8	0.2	90.6	90.4
689	16.13	0.2	103.9	103.65
686	17.05	0.3	111.6	111.35
683	15.3	0.2	93.8	93.55
680	14.99	0.3	90.7	90.4
678	14.67	0.3	84.3	84
675	15.81	0.3	97.1	96.75
673	16.5	0.4	104.7	104.35
670	17.09	0.3	109.5	109.25
668	17.98	0.2	121	120.75
665	16.81	0.3	112.8	112.45
663	16.26	0.4	108.5	108.15
660	15.92	0.3	108.4	108.15
658	15.64	0.2	104.1	103.8
655	14.79	0.4	97	96.7
652	16.06	0.2	110.3	110.05
649	14.7	0.3	94.1	93.8
647	15.31	0.3	104.2	103.85
644	16.72	0.4	119	118.6
641	15.6	0.4	105.6	105.2
638	15.31	0.4	102.3	102
635	16.15	0.2	113.2	113
633	16.3	0.2	113.5	113.3
630	15.68	0.2	107.5	107.1
628	14.32	0.6	91.9	91.4
625	14.44	0.4	91.8	91.45
623	14.49	0.3	95.4	95.05
620	14.5	0.4	96	95.6
618	15.19	0.4	105	104.65
615	14.77	0.3	102.7	102.3
613	14.5	0.5	101	100.55
610	15.49	0.4	111.6	111.15
608	15.21	0.5	111.4	110.85
606	16.92	0.6	130.1	129.6

Depth	Weight	Bkground	Raw LF	Adj. LF
601	15	0.4	106.7	106.4
599	14.89	0.2	105.5	105.2
597	15.28	0.4	111.1	110.65
595	14.58	0.5	107.5	106.95
592	15.41	0.6	120.9	120.2
590	14.87	0.8	109.9	109.2
588	14.93	0.6	107.1	106.5
585	15.87	0.6	118.5	117.8
583	15.74	0.8	118.4	117.6
581	14.92	0.8	109.6	108.8
579	15.62	0.8	119.2	118.45
576	15.28	0.7	99.2	98.45
574	14.15	0.8	77.2	76.3
572	14.73	1	94.6	93.65
570	15.69	0.9	104.8	103.85
567	15.58	1	104.1	103.7
566	15.95	-0.2	101.2	101.25
564	14.08	0.1	84.9	84.85
562	16.11	0	107.8	107.75
560	15.66	0.1	104.7	104.65
558	16.69	0	116.2	116.15
557	16.6	0.1	110.6	110.5
555	16.3	0.1	103.3	103.15
553	16.23	0.2	99.3	99.1
551	16.61	0.2	114.5	114.2
549	16.38	0.4	117.4	117
548	15.23	0.4	103.4	103.05
546	15.05	0.3	98.7	98.25
544	15.7	0.6	107.8	107.2
540	14.57	0.6	94.8	94.2
536	16.14	0.6	108.3	107.65
532	16.32	0.7	111.6	110.9
527	16.34	0.7	114.9	114.2
523	16.21	0.7	113.1	112.45
519	16.19	0.6	110.1	109.35
517	15.81	0.9	106.9	106
515	16.1	0.9	109.9	108.95
513	16.31	1	128.9	127.9
511	15.77	1	113.3	112.15